J. Earth Syst. Sci. (2020)129 88
https://doi.org/10.1007/s12040-020-1349-5

Petrology, geochemistry and geochronology of Neoarchean A-type granite from Alwar Basin, North Delhi Terrane, NW India

Arindam Misra*, Alok Chauhan and Debapriya Chatterjee

Geological Survey of India, Western Region, 15-16 Jhalana Dungri, Jaipur 302 004, India.
**Corresponding author. e-mail: arindammisra999@gmail.com*

MS received 20 June 2019; revised 24 November 2019; accepted 13 December 2019

A 2.53 Ga old Jhiri granite has been dated using zircon U–Pb systematics from the lowermost succession of North Delhi Terrane (NDT). The granite is an intrusive into the rocks of meta-volcano sedimentary sequence of basal Raialo Group of the Delhi Supergroup. Geochemically, the pluton is peraluminous, magnesian, alkali-calcic to alkali in character with strong negative anomaly for Ba, Ta, P and Ti and positive anomaly for K, Pb and Th. The plots on tectonic discrimination diagrams show the Jhiri granite to be of A-type with an affinity to the volcanic arc related granitoids. The comparison of Jhiri pluton with other Neoarchean granitoids of the Aravalli Delhi Mobile Belt (ADMB) and Bundelkhand craton shows the granite to be more evolved and have strong depletions for HREEs with $(La/Yb)_N$ >20. A hybrid source, having component of fractional crystallization-derived mafic melt mixing with melt generated by partial melting of early formed felsic crust in a back-arc extension or post-orogenic extension setting is proposed as the possible scenario for the generation and emplacement of Jhiri pluton.

Keywords. Jhiri granite; Neoarchean granites; A-type; North Delhi Terrane; Alwar Basin; age of Delhi sediments.

1. Introduction

Granites are an important tool in understanding evolution of earth crust over geological time. The granitic clan of rocks are the main constituent of the Archean cratons and their petrological, geochemical signatures along with isotopic studies provide the most direct evidences for the earliest crust formation and subsequent reworking. The plutons bear signatures of deep earth tectonomagmatic processes, which control the generation of melts along with their chemical characters. The change in magma chemistry also has been interpreted as a result of change in the protolith material as well as in tectonic settings (Chappel and White 1974). The term A-type granite was first introduced by Loiselle and Wones (1979) considering their specific chemical and tectonic environments exhibited by presence of anhydrous mineral phases in an anorogenic settings preferably in stable continental blocks and associated rift zones. Since the introduction of the term several type of granitoid plutons occurring in different tectonic settings has been clubbed within the broad A-type of rocks such as action of mantle plume or diapirism in an extensional regime (Emslie 1978; Morse 1982), thermal response to crustal thickening by earlier convergent plate tectonics (Van-Schmus and Bickford 1981) or post-collisional extension (Forster *et al.* 1997). The type and mechanism of

Published online: 04 March 2020

magma generation for such granitoid pluton is not well understood with some studies suggested direct fractionation from mantle derived mafic melts (Turner *et al.* 1992), whereas others favour for partial melting of early formed calc-alkaline crust at upper crustal level (Patiño Douce 1997) to residual granulites at lower crustal level (Collins *et al.* 1982; Whalen *et al.* 1987). The existence of A-type granitoids have been reported from as early as Late Archean to as young as Tertiary Period (Dall'Agnol *et al.* 2012) and hence, the study of their geochemical character with precise geochronology can provide important clues to the evolution of Precambrian crust through geological time. Moreover, identifying breaks in a meta-sedimentary sequence is difficult, due to obscured signatures during later deformations and/or absence of marker horizons. Since granites often intrude in such sequence or act as basements for such rocks, precise geochronology of intrusive plutons can provide a fairly well constrained relative age for the host or cover strata.

The Aravalli Delhi Mobile Belt (ADMB) exposes rocks of Archean to Neo-Proterozoic age. The northern part of the belt has been described as North Delhi Fold Belt (NDFB) by Sinha-Roy *et al.* (1998). The NDFB consists of rocks of Delhi Supergroup lying unconformably over a gneissic basement (Gupta *et al.* 1997). Later on, Singh *et al.* (2010) introduced the term North Delhi Terrane (NDT) and South Delhi Terrane (SDT) for describing the low grade meta-sedimentary sequence overlying the sialic basement rocks. They also proposed that ADMB to be a Proterozoic mobile belt consisting of a collage of NE–SW trending terranes juxtaposed along ductile shear zones. Crawford (1970) and Chaudhary *et al.* (1984) first published geochronological data on various granitoids of ADMB and reported presence of Archean granitoids (Untala Granite 2950 Ma, Berach Granite 2600 Ma) in the southern part of the ADMB. All these data were of whole rock Rb–Sr systematic which itself is error-chron and vulnerable to post-crystallisation alteration and metamorphism. Kaur *et al.* (2007 and reference therein) dated some of the intrusive granite plutons (Biharipur, Dabla, Jasrapura) of Khetri sub-basin lying in the northwestern corner of the NDT. The granitoids like Bairath, Dadikar, Harsora and Barodiya belonging to the Alwar sub-basin of NDT, have been dated by less reliable methods like zircon and monazite in EPMA by Biju-Sekhar *et al.* (2003) and whole rock Rb–Sr by Crawford (1970). Later on, Kaur *et al.* (2017) have carried out zircon U–Pb dating with more precise LA-ICP-MS method and have reported 1.71 Ga age for plutons of Alwar sub-basin. All these age data have postulated a widespread anorogenic acid magmatism in NDT during early Mesoproterozoic (Biju-Sekhar *et al.* 2003; Kaur *et al.* 2007, 2017) and have interpreted the granites to be basement to the Delhi metasediments, constraining the age of metasediments to be younger than 1660 Ma (Kaur *et al.* 2007). On the contrary, there are well preserved intrusive relations at least in case of Bairath and Barodiya pluton (Biju-Sekhar *et al.* 2003 in case of Bairath and authors' own observations) of Alwar sub-basin of NDT. The detrital zircon geochronological study carried out by Wang *et al.* (2017) has suggested the minimum depositional age of ca. 1720 Ma for Delhi metasediments which rejects the idea of Delhi sediments to be younger than 1660 Ma and also the hypothesis that the plutons acted as basements for Delhi sediments. Despite of all these studies, the chronological aspects between the cover rocks and the basement complex and also within the cover rocks are less understood due to paucity of age data and post-sedimentation complex deformational history. The studied granitoids and the associated metasediments show that there is a gap in understanding over the timing and phases of felsic plutonism in NDT and also their interrelation with the surrounding metasediments. Moreover, recent geochronological studies of the cover rocks across NDT and SDT show a distinct much older age for the NDT and thus questioning their stratigraphic correlation and geological milieu (Mckenzie *et al.* 2013; Wang *et al.* 2017). In this study, we report for the first time existence of 2529.6 Ma old A-type granite in the Alwar basin of NDT along with its petrology and geochemical characteristics. The existence of older granitoid pluton within the cover rocks (Delhi Supergroup) reflects a new understanding of the basement-cover relationship within the NDT.

2. Geological setting

2.1 *Regional geological setting*

The northwestern part of Rajasthan exposes folded sequences of the ADMB extending from near Delhi in the north to beyond Champaner in the south covering states of Delhi, Haryana, Rajasthan and

Gujarat. The Proterozoic ADMB rests over cratonic basement rocks of Archean age. Heron (1917, 1922) classified the rocks of the area into three broad, but distinct groups. In his classification, the Archean basement rocks have been grouped as Banded Gneissic Complex (BGC) and the Proterozoic cover sequences have been grouped as Aravalli and Delhi Supergroup. Later on, Sinha-Roy *et al.* (1998), based on the physical continuity of rocks and distinct magmatic histories, have subdivided the rocks of Delhi Supergroup into two domains, the North Delhi Fold Belt (NDFB) and South Delhi Fold Belt (SDFB). The work carried out by Singh *et al.* (2010) has suggested the term NDT and SDT considering the collisional tectonics of ADMB where different terranes have juxtaposed along regional shear zones. Apart from the dominance of meta-sedimentaries, the rocks of the Aravalli and Delhi Supergroup are having evidences of igneous activities of both volcanic and plutonic in character. The NDT which consists of rocks exposed north of Ajmer city, Rajasthan and continues up to Delhi with a strike length of more than 300 km bears evidences of acidic igneous activity in the form of intrusive plutons of granitic clan. The earlier works done by various workers have sub-divided the northern part into three sub-basins namely Khetri in the west, Alwar in the centre, whereas Lalsot-Bayana sub-basin in the east (Sinha-Roy *et al.* 1998), and further suggested a three-tier stratigraphic classification, Raialo Group, Alwar Group and Ajabgarh Group for the Delhi Supergroup of rocks. Singh (1988) studied the sedimentary pattern and palaeo-environment of the Delhi metasediments and suggested that unconformity based three groups, the Raialo, the Alwar and the Ajabgarh deposited within graben or half-graben like structures in a rift setting.

2.2 *Geology of the study area*

The study area falls within southern part of the Alwar sub-basin of NDT and is dominated by metamorphosed volcano-sedimentary rocks of Delhi Supergroup (figure 1). The first generally accepted stratigraphic framework was given by Heron (1917) where the rocks were divided into two distinct groups, Pre-Delhi System and Delhi System. The Delhi System was then subdivided into Raialo Series, Alwar Series, and Ajabgarh Series. The Raialo Series of rocks were marked as unconformity bounded successions with presence of unconformity at the top as well as at the bottom. Later, three tier lithostratigraphy of the area was published by Geological Survey of India (2001) where the lowermost Raialo Group is represented by calcareous and areanaceous package at the base followed by basic volcanics and associated meta-sedimentaries known as the Tehla Formation at the top. The middle Alwar Group is dominated by quartzite along with intermittent basic flows near to the base, whereas the upper Ajabgarh Group is dominated by argillaceous and calcareous sediments. Singh (1988) stated an evolving intracratonic rift model for interpreting the inter-relationship between the sedimentary facies and palaeo environment and opined that it is comparable with many other intracratonic rift basins of the world. The available geochemical data of the granitoid plutons from these basins also support this view considering their interpreted anorogenic character (Biju-Sekhar *et al.* 2003; Kaur *et al.* 2007). Later study carried out by Kaur *et al.* (2017) has interpreted the plutons to be emplaced in post-collisional extension settings.

The Raialo Group consists of quartzite of Tehla Formation exposed near northwestern contact of Jhiri granite, whereas the eastern contact is with impure marble of Dogeta Formation (figure 3). Polyphase deformation in the Alwar sub-basin has resulted into complex outcrop patterns. The rocks are folded into appressed upright to isoclinal shallow to moderate plunging NNE–SSW trending antiforms and complementary synforms, which were subsequently refolded on NW–SE and ENE–WSW axial planes, resulting in axial culminations and depressions. The intrusive bodies in the area are in the form of sills and dykes in case of mafic bodies, whereas acidic rocks are in the form of granitic pluton of variable shape with sharp contact with the surrounding meta-sediments. At many places, the intrusive granitoids (Barodiya, Bairath, Harsora) lie at the core part of the regional antiform (figure 2). In this study Jhiri granite, lying in the SE part of Alwar sub-basin has been studied.

3. Dataset and methodology

3.1 *EPMA*

Mineral composition and morphological character of silicate minerals was determined using CAMECA SX-100 electron microprobe at EPMA

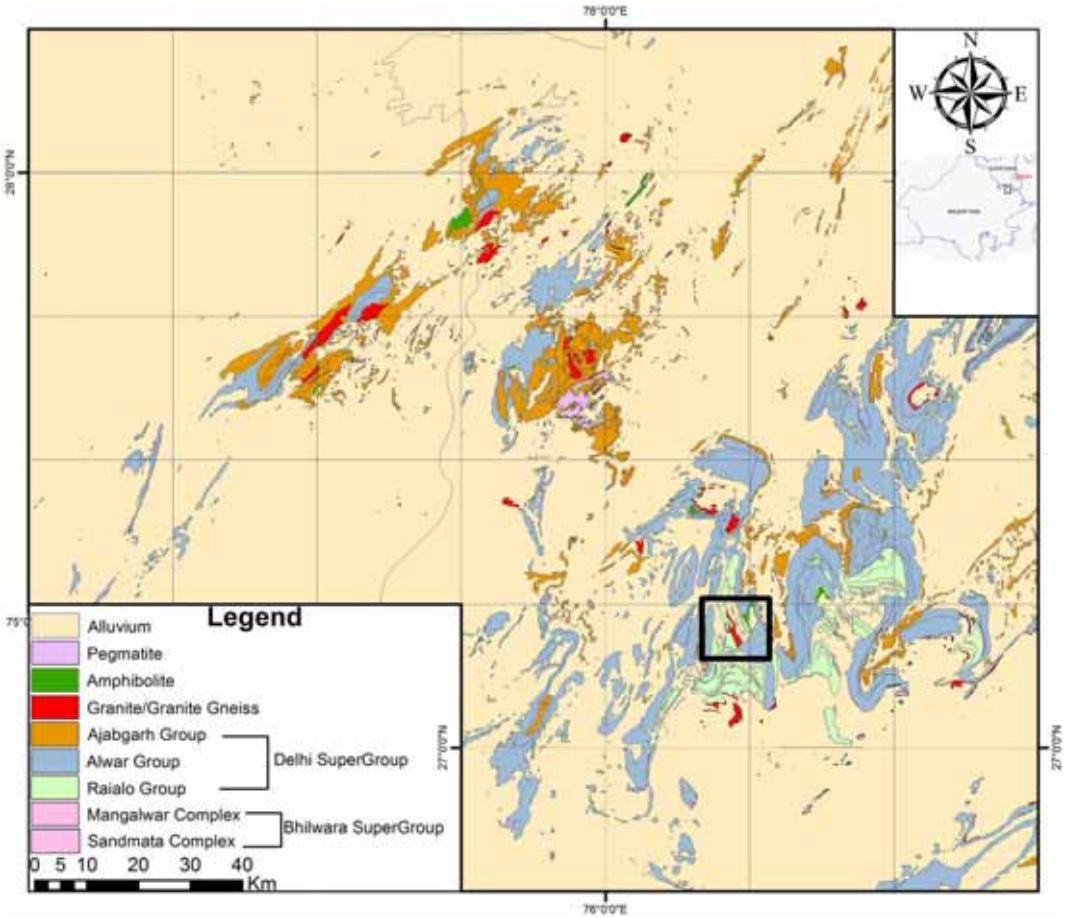

Figure 1. Regional geological map showing major lithostratigraphic units of North Delhi Terrain prepared using 1:50 K geological database of GSI. Study area is shown by square.

Laboratory, Geological Survey of India, Bangalore, India. The electron microprobe is equipped with four spectrometers and an EDS detector. The analytical condition for silicate minerals were maintained through accelerating voltage of 15 kv and current 15 nA with peak counting times of 30 s for all elements. The beam size for the analysis is 1 μm. All standards used for calibration of the instrument are natural standards. The silicate minerals were analyzed with the following standards: Jadeite (Na Kα), Wollastonite (Si Kα, Ca Kα), Olivine (Mg Kα), Corundum (Al Kα), Orthoclase (K Kα), Rutile (Ti Kα), Cr_2O_3 (Cr Kα), Rhodonite (Mn Kα) and Fe_2O_3 (Fe Kα). The spectrometer conditions for the analyses were as follows: Sp1 TAP, Sp4 TAP, Sp2 PET, Sp4 TAP, Sp1 TAP, Sp2 PET, Sp3 LPET, Sp3 LPET and Sp5 LIF. The data reduction procedure was performed by using ZAF correction. The analytical error for major elements is $< 1\%$. A total of 47 nos. of spot analyses have been carried out from two samples.

3.2 *Whole rock chemistry*

The major and trace elements for the Jhiri pluton were analysed by X-ray fluorescence (XRF) spectrometry on fused glass discs and powder pellets, respectively, at the Regional Chemical Laboratory of Geological Survey of India, Western Region, Jaipur using an XRP AXIOS, Panolytics, Wetherl and fluorescence spectrometer. The relative error is better than 1% for major elements and 0.8–6% for trace elements, depending on their concentrations. Rare earth elements (REE) were determined with ICP-MS at the Regional Chemical Laboratory of Geological Survey of India, Western Region, Jaipur using ELAN DRC-e, PERPIN Elmer ICP-MS. A total of six samples have been analysed.

3.3 *Geochronology*

For geochronological study, ∼5 kg (–60 mesh to +80 mesh sizes) powdered samples of the granite were processed to separate heavy minerals like

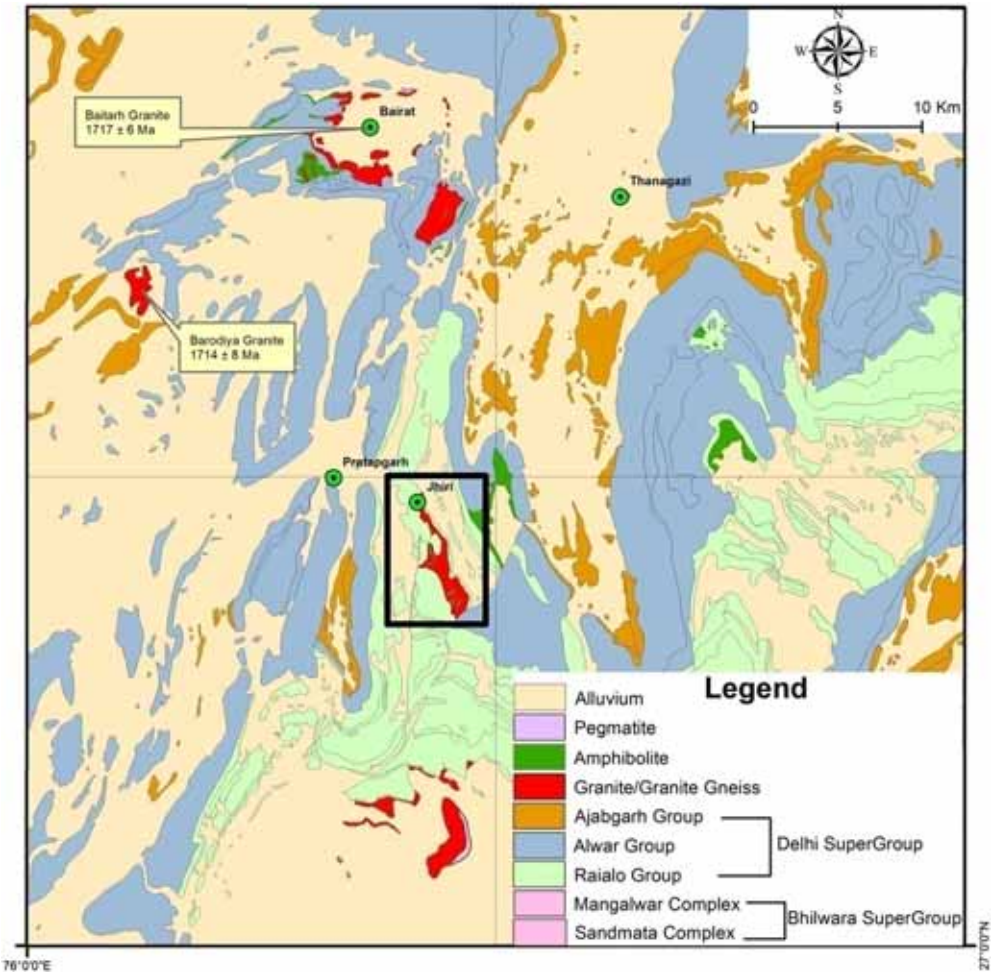

Figure 2. Geological map of parts of Alwar Basin showing major rock units with intrusive granitic plutons and their absolute ages. The ages of Bairath and Barodiya pluton are zircon U–Pb age after Kaur *et al.* (2017). The location of Jhiri granite is marked with rectangle.

zircon for U–Pb zircon study. The powdered fractions were panned under a stream of water repeatedly to get rid of the finer and lighter fractions and then dried under infrared lamp. Heavies were separated from this fraction by density separation using Wilfrey table followed by separation by heavy liquid (bromoform). Further separation of heavies was done in Frantz Isodynamic separator. The obtained fraction was cleaned with isopropanol and allowed to dry under infrared lamp. The zircon crystals were then handpicked under binocular microscope. A split of about 20–35 well developed, unaltered zircon crystals were selected and incorporated into a 1-inch diameter epoxy mount (figure 8). The mount was sanded down till the grain faces are surfaced and then polished (figure 9a, b). Prior to isotopic analyses, the grain surfaces within the mounts were initially cleaned with 2% HNO_3 followed by de-ionized water and dried in vacuum oven in ultra clean conditions.

U–Pb isotopic analyses were carried out in Laser Ablation (LA) Multi-Collector (MC) Inductively Coupled Plasma Mass Spectrometry (ICPMS), viz., (LA-MC-ICPMS). The analyses involved ablation of zircons with a New Wave 193 Excimer Laser by static ablation (spot analyses). The ablated material was carried into the plasma source of Nu-II multi-collector ICPMS by ultrahigh grade helium gas. Operating conditions of measurement are tabulated (table 4). Prior to analysis, common Pb (non-radiogenic natural ^{204}Pb) correction was done following standard measurement protocol (White *et al.* 2000; Horstwood *et al.* 2003) by measuring ^{204}Pb and assuming an initial Pb isotopic composition from Stacey and Kramers (1975). ^{204}Hg generally masks ^{204}Pb during mass spectrometric analyses. However, the masking syndrome had been taken care of by a low 206/204 ratio. All measurements were made in static mode, using combination of faraday detectors with

10^{11} Ohm resistors for ^{238}U, ^{232}Th, ^{208}Pb and ion counting channels for ^{207}Pb, ^{206}Pb and ^{204}Pb. Samples have been analysed in standard-sample-standard bracketing method in time resolved analyses (TRA) mode. Every 4–5 unknown zircons have been bracketed with known standards. The size of the ablation pit varies from 30–35 micron in diameter maintaining an aspect ratio of 2:1. Standards used during the above analyses were 91500 (ID-TIMS age of 1062 ± 0.8 Ma; 2-sigma, Wiendenbeck *et al.* 1995) and Plesovice (337.13 ± 0.3 Ma; Sláma *et al.* 2008) and all the results are well within the accepted analytical uncertainties. The raw data has been exported to Iolite 2.5 for necessary data reduction processes (Paton *et al.* 2010) that includes corrections for baseline, instrumental drift, mass bias and down-hole fractionation.

4. Result

4.1 *Mapping and field characteristics*

The Jhiri granite is located about 8 km east of Pratapgarh village and about 25 km SSW of tehsil town Thanagazi (figure 2). The exposed area of the granite is about 5 km^2 and shows a linear outcrop pattern in geological map (figure 2). The map (figure 3) of the detailed study area shows the granite pluton share intrusive contact with the schistose rocks (meta-basic volcanics) of Tehla Formation of Raialo Group. The contact between the schistose (Tehla volcanics) rocks and the overlying quartzite is sharp with the presence of a quartz pebble conglomerate (QPC) zone near the western contact (figure 4a, f). The schistose rocks are mostly quartz-tremolite bearing actinolite schist with development of biotite at places. The Jhiri pluton shows intrusive relations with the schistose unit (figures 4a, 5a). Well preserved intrusive contact are present at places; near to the western and eastern contact (figure 4b, c). The western contact of the granite contains rafts of surrounding schistose rocks which are part of the country rock and thus proving its unequivocal evidence for intrusive nature (figure 5b). At places away from the contact zone few centimetres long, fragments of schistose rocks are preserved with diffused contact zones within the Jhiri granite (figure 5h). Along the western contact the granites occupy the lower ground whereas the metasedimentary package consists of schistose counterpart of Tehla meta-volcanics, minor impure marble bands and quartzites of Raialo Group form the hillocks. The contact between granite and associated schistose rocks shows presence of thin zone of feldspathization (figure 5c). Development of feldspar crystals is observed within the host schistose rocks near to the contact suggesting intrusion of hot granitic magma which triggered some chemico-physical changes within the host rocks near the contact zone. The presence of such zone supports the view of the intrusive nature of the granite which otherwise will be absent in case it acted as a basement to the meta-volcano-sedimentaries. The eastern contact lies with partly exposed feldspathic quartzite and impure marble rocks of Dogeta Formation of Raialo Group.

The Jhiri granite is dark grey colour in fresh surface and is moderately crystalline. It is porphyritic at places with size of phenocrysts varying from few millimetres to up to 3 cm (figure 5d). The phenocrysts are euhedral in shape and mostly composed of alkali feldspar. The ground mass contains mostly feldspar (plagioclase and alkali both) and quartz with mafic minerals in the form of biotite and muscovite. The rock contains significant amount of biotite which gives the dark grey colour of the pluton in outcrop. Evidences of deformation in the form of development of foliation planes are also observed. At few places the phenocrysts show alignment parallel to the foliation indicating deformation in a semi-solid state (figure 5e). The magmatic lineation as evidenced by the alignment of early formed feldspar phenocrysts is preserved at many places within the pluton (figure 5f). Some of the phenocrysts show grain boundary reduction and rounding off of early formed euhedral phenocrysts (figure 5g). Emplacement of silica veins of different stages has also been observed.

4.2 *Petrographic study*

Petrographic study using thin sections shows presence of alkali and plagioclase feldspar, quartz and biotite as the major constituent minerals, whereas accessory phases like muscovite, apatite, zircon and epidote are also present. The phenocrysts are mostly alkali in composition, whereas the groundmass shows presence of both alkali and plagioclase (figure 6a). Some of the alkali feldspar phenocrysts show perthitic character. The groundmass constitutes smaller crystals of quartz,

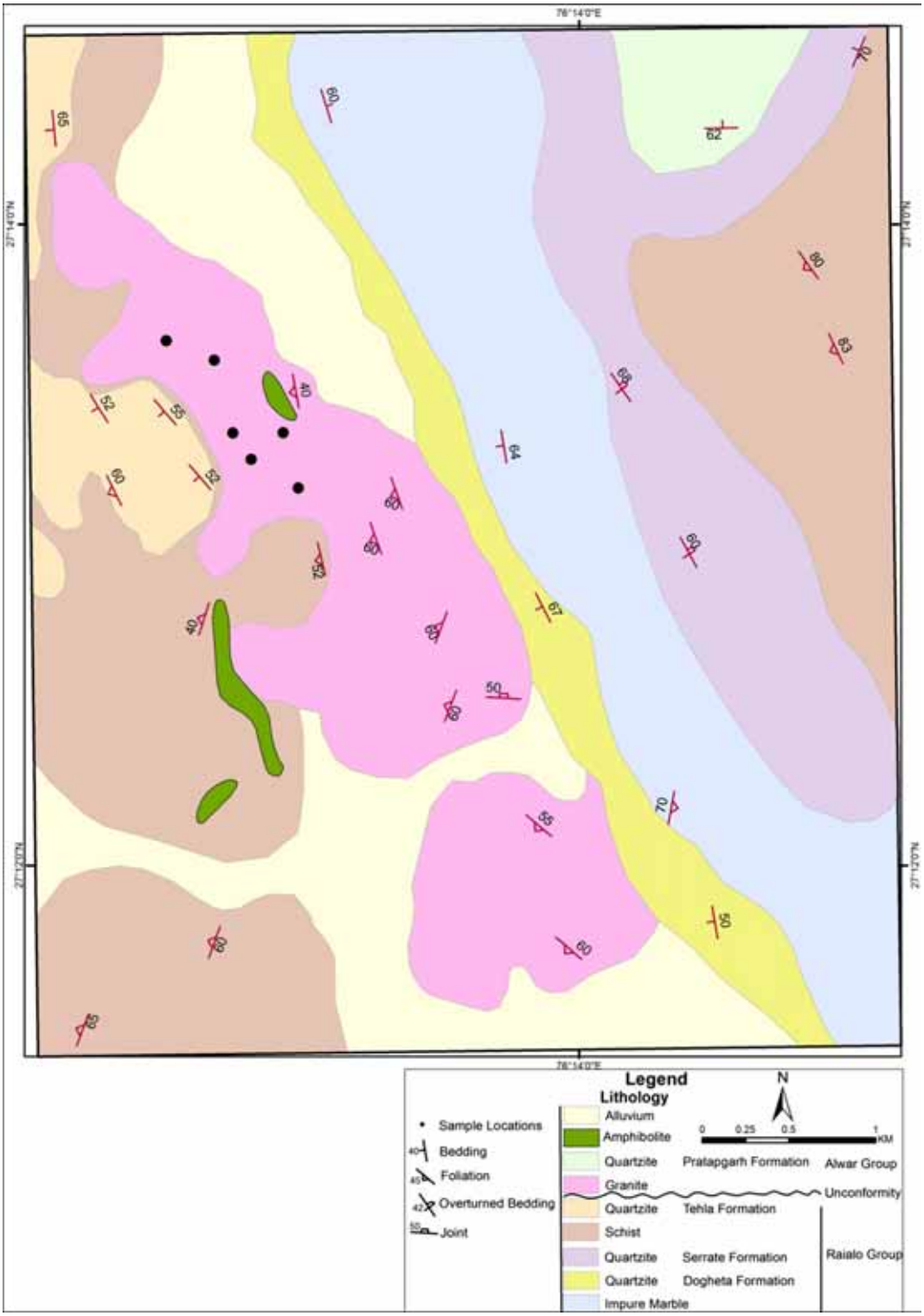

Figure 3. Detailed geological map of Jhiri pluton with location of sample points for geochemical, geochronological as well as modal analysis study.

alkali and plagioclase feldspar along with biotite and muscovite (figure 6b). The plagioclase crystals occurring in the groundmass have vermicular quartz crystals within larger crystals of plagioclase feldspar, forming myrmekitic intergrowth (figure 6c). Often the myrmekites occurs near to the contact with microcline megacrysts and extend towards the microcline grain boundaries (figure 6c) which can be explained by successive replacement of plagioclase by microcline (figure 6b). The K-rich

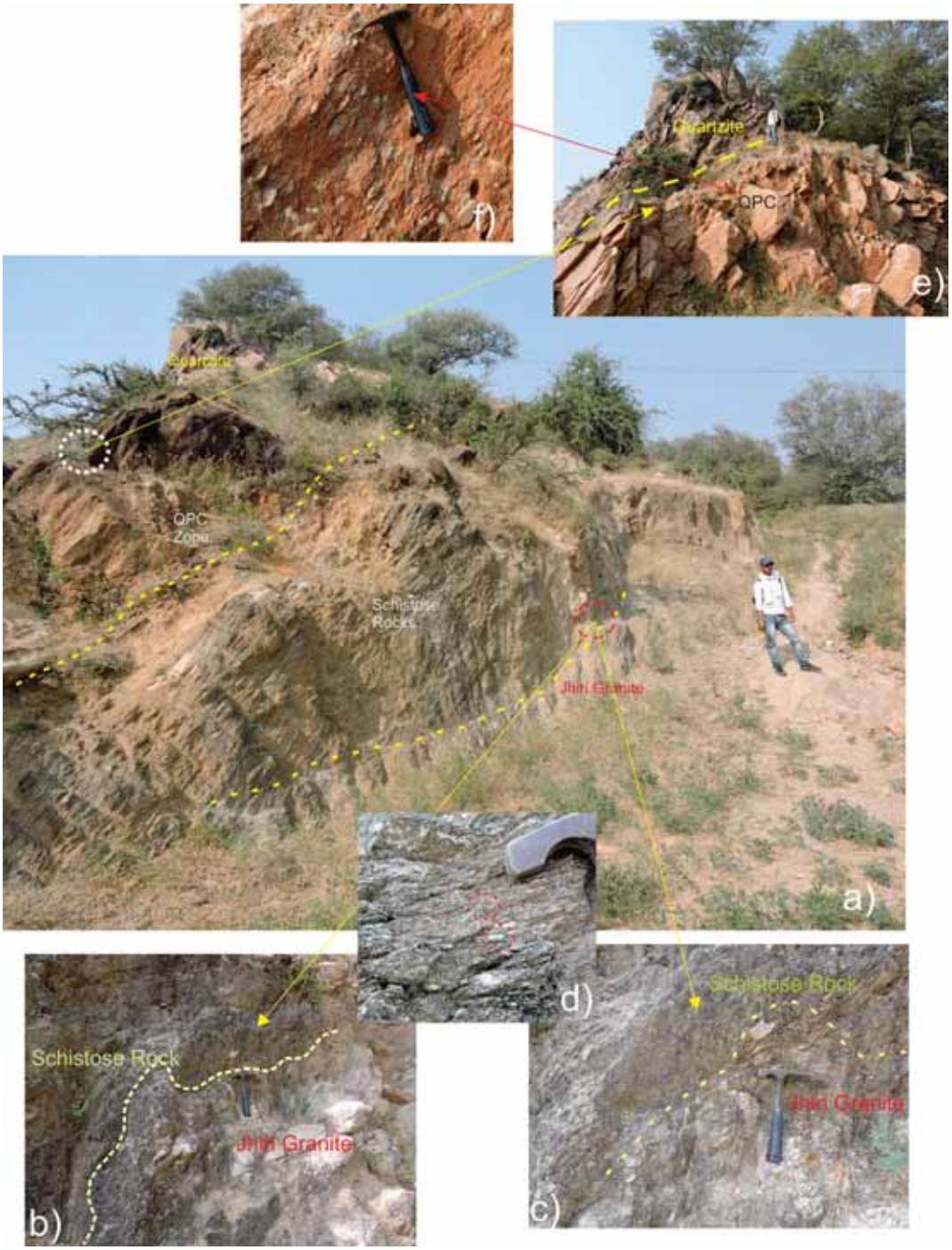

Figure 4. Juxtaposition of different lithounits and their interrelation at the western contact of Jhiri pluton with the cover sequence; the view of the observer is towards NW; (**a**) intrusive contact of Jhiri granite with the host schistose rocks along with position of QPC and schistose rocks; (**b** and **c**) tongues and apophyses of Jhiri granite; (**d**) close-up view of the schistose rocks having euhedral crystals of alkali feldspars near to the contact zone; (**e**) sharp contact between QPC zone and the overlying quartzite showing orientation of lithounits in the area; (**f**) close-up view of the QPC unit in the study area.

fluid can migrate through the micro-fractures and replaces the early formed plagioclase. Both biotite and muscovite are present in the groundmass (figure 6d). The contact between biotite and muscovite is sharp and often occupy the spaces between two feldspar crystals or occur near to the boundary of large feldspar crystals. The other accessories are mostly zircon and apatite with rare occurrence of sphene and fluorite (figure 6e). The zircon crystals occur in association with biotite and muscovite rich zones or the intergranular spaces of quartz crystals. The opaques are mostly magnetite

Figure 5. Field photographs of Jhiri granite. (**a**) photographs showing intrusive contact of Jhiri granite with host schistose rocks of Raialo Group; (**b**) Rafts of schistose rocks of Raialo Group within Jhiri granite near to the western contact; (**c**) Presence of thin zone of feldspathization near to the contact of Jhiri granite with the schistose rocks; (**d**) Photographs of randomly oriented euhedral feldspar crystals in grey coloured matrix of Jhiri granite; (**e**) Photographs showing alignment of early formed phenocrysts of Jhiri granite suggesting evidence of crystal-plastic deformation; (**f**) Photographs showing development of mineral lineation by linear distribution of early formed feldspar phenocrysts; (**g**) Photographs of post-crystallisation deformation and rounding off of early formed phenocrysts of Jhiri granite; (**h**) Photographs of undissolved clasts of schistose rocks within Jhiri granite showing development of sharp margin and formation of feldspar phenocrysts near margin.

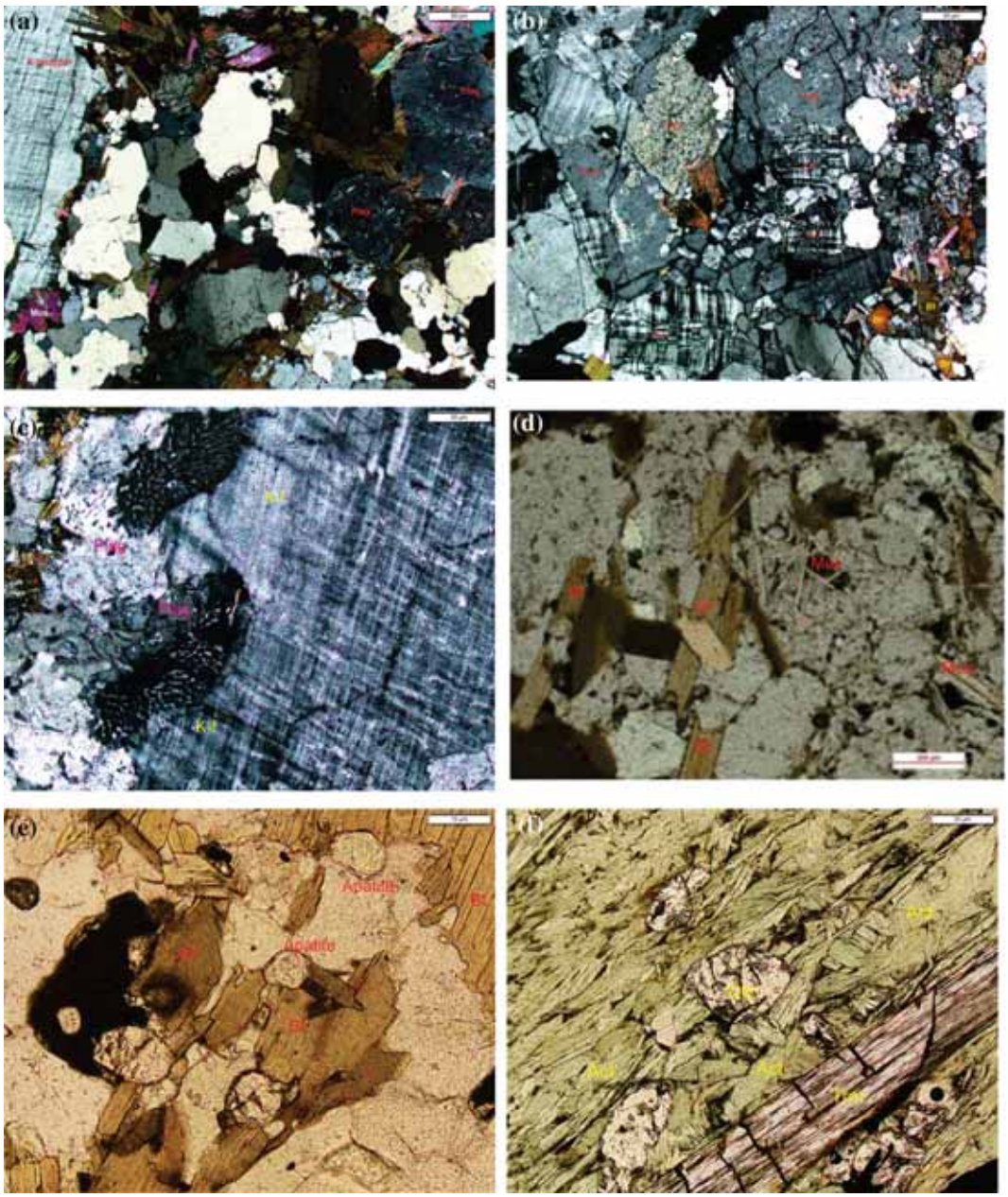

Figure 6. (**a**) Photo micrograph of Jhiri granite showing K-feldspar phenocryst and groundmass having quartz, plagioclase, biotite and muscovite; (**b**) Photomicrograph of Jhiri granite having two feldspar composition in the groundmass. The plagioclase feldspars are being replaced by development of microcline; (**c**) Photomicrograph showing presence of warp like quartz crystals resulting myrmekitic texture near to the boundary of large microcline crystals. The replacement front of plagioclase by microcline is also evident by the convex upward grain boundary of microcline; (**d**) Photomicrograph of Jhiri granite showing its two mica character with presence of biotite and primary muscovite; (**e**) Photomicrograph showing presence of apatite as accessory mineral within Jhiri granite in association with biotite; (**f**) Photomicrograph of the host schistose rocks (metabasic volcanics) having actinolite as major constituent and associated tremolite and quartz.

along with ilmenite and pyrite. Petrographic study of the schistose rock near the contact zone shows actinolite as the major mineral along with presence of minor quartz and tremolite (figure 6f).

The modal composition of the granitoid pluton has been calculated and plotted in the QAP plot after Streckeison (1976). A total of 300 counts have been calculated for each sample with Quartz (Q), Alkali Feldspar (A), Plagioclase (P), Biotite (Bt), Muscovite (Mus) and others (Acc) as different classes (table 2). The obtained counts were then converted to percentage values in which the Q, A and P values were again recalculated and have been used for plotting. The plots show

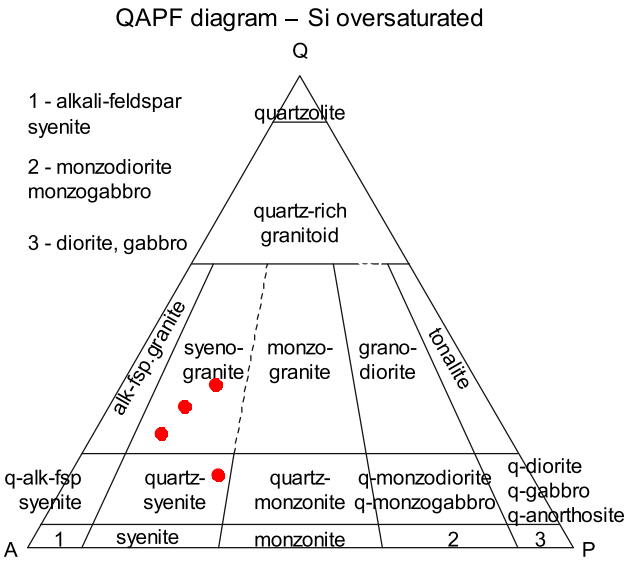

Figure 7. Modal composition of Jhiri granite plotted on QAP diagram of Streckeison (1976). The plots show the composition varies from Syeno granite to Quartz Syenite field.

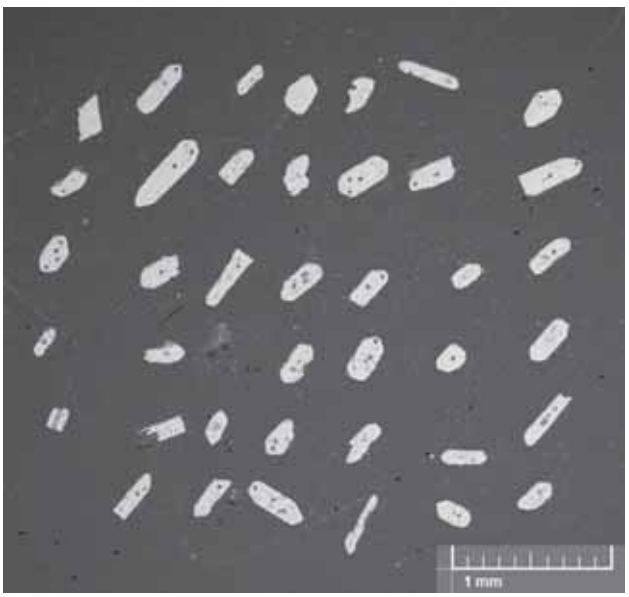

Figure 8. Back Scattered Electron (BSE) image of the studied zircon mount used for U–Pb dating of Jhiri granite.

mineralogical composition of the granitoid varies from Syeno-granite to Quartz-syenite variety (figure 7).

4.3 *Mineral chemistry and petrochemistry*

4.3.1 *Mineral chemistry*

The mineral chemical data of Jhiri granite has been studied using EPMA techniques and by analyzing the chemistry of the major as well as accessory phases. EPMA analysis of two representative samples has been carried out to understand the phenocrystic and groundmass phases.

4.3.1.1 *K-feldspar:* The analysis of potash feldspar crystals shows their composition ranges 13% to more than 16% in case of K_2O, whereas the Na_2O concentration varies from 0.5% to 2% (table 1). The orthoclase (Or) content varies from 81% to 96% whereas the albite (Ab) content ranges from > 3% to 18%. The general compositional range for K-feldspar crystal occurring both in groundmass as well as in phenocrystic phase is $Or_{96\text{-}81}Ab_{4\text{-}19}$. The compositional plot of the k-feldspar crystals show them to be plotted in the sanidine field (figure 10). The comparison between the phenocrystic k-feldspar with the groundmass k-feldpar phases show a close range of Or content (92–93) for the crystals occurring in the groundmass whereas the phenocrysts have a wide range of Or (81–96).

4.3.1.2 *Plagioclase:* The plagioclase crystals mostly occupy spaces in the groundmass composition. The analysis of plagioclase crystals shows relative enrichment in Na_2O compared to CaO. The Na_2O percentage varies from > 8% to 11%, whereas the CaO content varies from 0.5% to >4%. The general compositional range for plagioclase crystals occurring both in groundmass as well as in the core part of phenocryts is $Ab_{97\text{-}78}An_{3\text{-}21}$. The compositional plot of the plagioclase crystals show most of them plotted in the oligoclase field, whereas two of them are plotted in the albite field (figure 11). The comparison of the groundmass plagioclase with the phenocrystic core show a close range of Ab (81–83) in the phenocrystic core compared to the groundmass Ab (79–97). The plots also show two of the analysed feldspar from the groundmass phase as albite ($Ab_{93\text{-}97}$). Presence of albite in the ground mass suggests a later enrichment of Na in the system compared to Ca resulting crystallization front shifted towards soda end in a Ab–An system.

4.3.1.3 *Biotite:* A total of nine analyses were carried out of biotite crystals. The MgO content of biotite varies in a close range of 7.5% to 8.1%, whereas the FeO content is > 20%. The X_{Mg^*} values calculated for the analysed biotite range from 0.37 to 0.39 showing Mg poor nature, whereas the X_{Fe^*} values range from 0.61 to 0.63

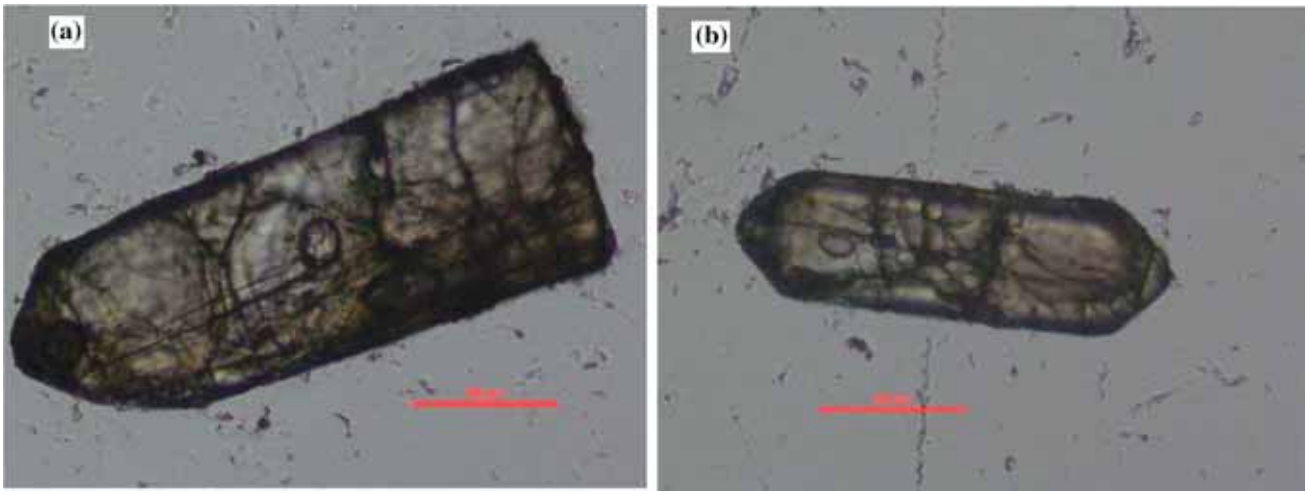

Figure 9. Photographs of representative polished zircon (**a** and **b**) of Jhiri granite.

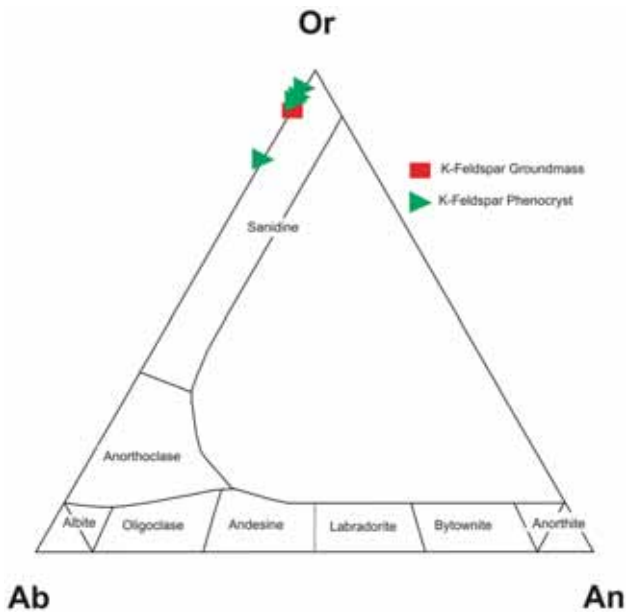

Figure 10. K-Feldspar composition plot for the Jhiri granite show all data points plot in sanidine field and rich in orthoclase.

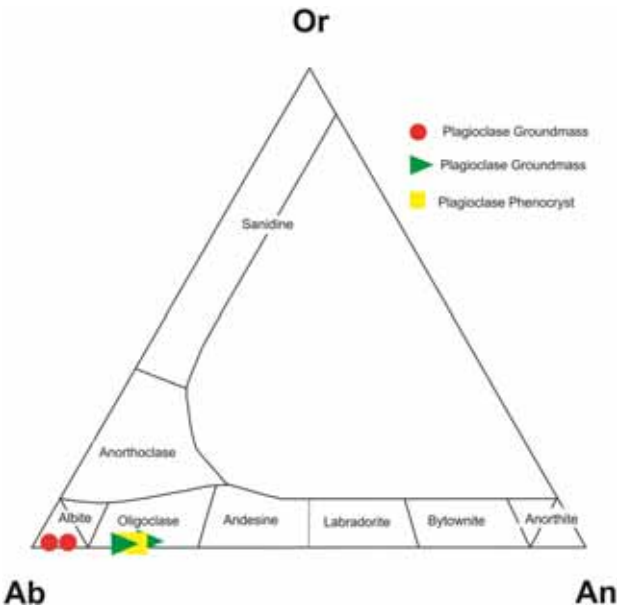

Figure 11. Plagioclase composition of Jhiri granite falling in albite-oligoclase field. The composition of groundmass and phenocryst core falls in the oligoclase field.

suggesting enrichment in iron. The narrow range of the $Fe^{2+}/(Fe^{2+}+Mg)$ suggests their magmatic nature. TiO_2 content varies from 2 to 2.67% with Ti cations vary between 0.26 and 0.33 apfu in the analysed biotites. Total Al and Fe/(Fe + Mg) variables are commonly used to illustrate compositional relationships of trioctahedral micas from igneous rock suites. The analytical data plotted in the classification diagram proposed by Deer *et al.* (1996) show them to be of annite variety with enrichment of Fe (figure 12). The calculated cation of the biotite crystals were then plotted in biotite classification diagram proposed by Foster (1960) for trioctahedral biotites. The data plot in the Ferrous Biotite (Fe^{2+}) field (figure 13). The ASI ($Al_2O_3/(CaO + Na_2O + K_2O)$) value of biotite has been calculated and ranges between 1.6 and 1.7 suggesting increased alumina activity in the magma.

Abdel-Rahman (1994) suggested discrimination diagrams on the basis of major elements (FeO, MgO, Al_2O_3) of biotites in igneous rock crystallized from A, P and C magma types. Based on this classification, biotites in anorogenic alkaline suites

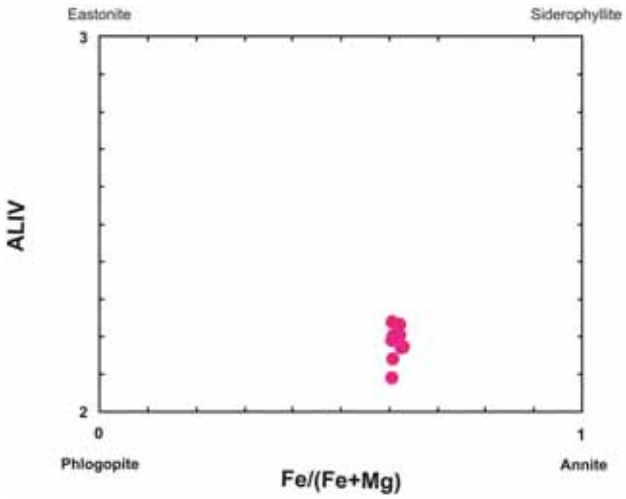

Figure 12. Biotites of Jhiri granite plotting in the annite field with Fe enrichment, after Deer *et al.* (1996).

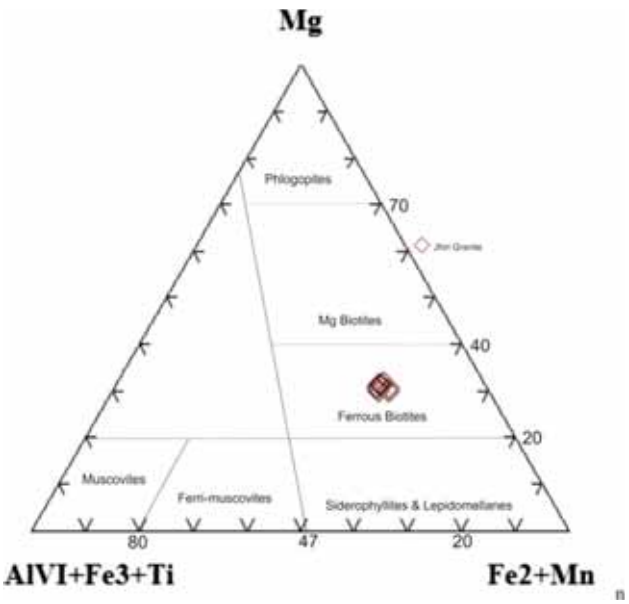

Figure 13. Biotite plot of Jhiri granite after Foster (1960) shows them to be of ferrous biotite character.

(Field A) are mostly iron-rich and siliceous biotites (near annite) with an average FeO/MgO ratio of 7.04; those in peraluminous (including S-type) suites (Field P) are siderophyllitic in composition and have an average FeO/MgO ratio of 3.48; whereas biotites in calc-alkaline orogenic suites (Field C) are moderately enriched in Mg; with an average FeO/MgO ratio of 1.76. The Jhiri granite shows the FeO/MgO values range from 2.7 to 3, suggesting affinity to the peraluminous character. The analytical data of biotites of Jhiri pluton have been plotted in these four diagrams and lie near to the calc-alkaline and peraluminous boundary with most of them falling within peraluminous field (figure 14).

4.3.1.4 *Muscovite:* The analyses of muscovite crystals in the Jhiri pluton show higher concentration for TiO_2, MgO and lower concentration of FeO and Na_2O. Miller *et al.* (1981) determined some textural criterion for identification of primary muscovite from secondary one, such as coarser grain size comparable to primary phases, cleanly terminated with subhedral to euhedral grain boundary and have clean, unaltered, igneous texture. The petrographic study suggests these entire criterions are valid for muscovites of Jhiri granite. Miller *et al.* (1981) also studied the paragenesis of plutonic muscovite; since the presence of primary muscovite is considered significant in respect of magma composition and depth of crystallization. Their study showed a significant enrichment of TiO_2, Al_2O_3 and Na_2O in case of primary muscovite compared to the secondary one. Comparison of the values of primary muscovite chemistry from Miller *et al.* (1981) with that of the studied granite show a significant enrichment of TiO_2 and depletion of Na_2O in case of Jhiri granite. The higher TiO_2 values indicate towards the primary nature of the muscovite crystals. The plot of muscovite mineral data in the diagram proposed by Miller *et al.* (1981) shows the analysed muscovites fall in the primary muscovite field (figure 15). The ASI value ($Al_2O_3/(CaO + Na_2O + K_2O)$) calculated for muscovite varies from 2.66 to 2.73.

4.3.2 *Petrochemistry*

4.3.2.1 *Major oxide chemistry:* Six samples of the pluton were analysed and show silica concentration ranging from 64% to 68%, suggesting a less evolved nature (table 2). The K_2O and Na_2O content of the samples vary from 0.7% to > 6% and 2% to > 7%, respectively. The K_2O/Na_2O value shows a wide range starting from 0.1 to 2.9. The results of the major oxides were then recalculated to 100% in order to carry out CIPW NORM calculation and other geochemical plotting purposes. Since the granite is rich in biotite, a hydrous phase, the major oxide analysis showed a high proportion of LOI (table 2). The CIPW NORM calculation shows the granite to be rich in alkali feldspar with a normative percentage of >50% and poor in quartz 30%<. The rock has normative hypersthene, rutile, apatite, hematite and ilmenite. The analysed

Table 1. *Mineral chemistry data of Jhiri granite (oxide values in wt%).*

Sample no.	JHG1/ TS15	JHG1/ TS15	JHG1/ TS15	JHG1/ TS15	JHG1/ TS15	JHG1/ TS15	JHG1/ TS15	JHG1/ TS15	JHG1/ TS15	JHG1/ TS15	JHG1/ TS15	JHG1/ TS15	JHG1/ TS15
Mineral	K–f	K–f	K–f	K–f	K–f	K–f	K–f	Plag	Plag	Plag	Plag	Plag	Plag
Analysis	1/1	2/1	25/1	26/1	6/1	7/1	8/1	14/1	2/1	22/1	30/1	31/1	39/1
Location	phen	phen	gmass	gmass	phen	phen	phen	gmass	gmass	gmass	gmass	gmass	gmass
SiO_2	64.13	63.71	63.89	62.94	63.75	63.55	64.14	66.19	67.51	63.03	63.06	62.58	62.62
TiO_2	0.02	0.01	0.02	0.03	0.01	0	0.03	0.07	0.01	0	0	0	0.02
Al_2O_3	18.2	18.28	18.49	18.38	18.36	18.1	18.15	20.69	19.9	23.03	22.7	23.1	23.1
Cr_2O_3	–	–	–	–	–	–	–	–	–	–	–	–	–
FeO	0	0	0.06	0.05	0.05	0	0	0.17	0.12	0.09	0.09	0	0
MnO	0	0	0	0	0	0	0.03	0.07	0	0.02	0.07	0	0.02
MgO	0	0.01	0.03	0.06	0.05	0	0.03	0	0	0	0	0	0
CaO	0	0	0.04	0	0.01	0	0	1.32	0.59	4.03	4.26	4.23	4.51
Na_2O	2.09	0.56	0.89	0.79	0.42	0.7	0.62	10.84	11.28	9.31	9.04	9.21	9.1
K_2O	13.92	15.69	15.49	15.56	16.07	15.52	15.81	0.08	0.11	0.09	0.09	0.15	0.17
Sum	98.36	98.26	98.91	97.81	98.72	97.87	98.81	99.43	99.52	99.6	99.31	99.27	99.54
Oxygen	32	32	32	32	32	32	32	32	32	32	32	32	32
Si	11.974	11.97	11.929	11.9	11.946	11.985	11.991	11.686	11.872	11.188	11.224	11.152	11.139
Al	4.002	4.045	4.066	4.093	4.052	4.02	3.996	4.302	4.121	4.814	4.758	4.848	4.839
Fe_3	0	0	0	0	0	0	0	0	0	0	0	0	0
Ti	0.003	0.001	0.003	0.004	0.001	0	0.004	0.009	0.001	0	0	0	0.003
Fe_2	0	0	0.009	0.008	0.008	0	0	0.025	0.018	0.013	0.013	0	0
Cr	–	–	–	–	–	–	–	–	–	–	–	–	–
Mn	0	0	0	0	0	0	0.005	0.01	0	0.003	0.011	0	0.003
Mg	0	0.003	0.008	0.017	0.014	0	0.008	0	0	0	0	0	0
Ca	0	0	0.008	0	0.002	0	0	0.25	0.111	0.766	0.812	0.808	0.86
Na	0.757	0.204	0.322	0.29	0.153	0.256	0.225	3.711	3.846	3.204	3.12	3.183	3.139
K	3.316	3.761	3.69	3.753	3.842	3.734	3.771	0.018	0.025	0.02	0.02	0.034	0.039
Sum	20.052	19.984	20.035	20.065	20.018	19.995	20	20.011	19.994	20.008	19.958	20.025	20.022
Ab	18.6	5.1	8	7.2	3.8	6.4	5.6	93.3	96.6	80.3	78.9	79.1	77.7
An	0	0	0.2	0	0.1	0	0	6.3	2.8	19.2	20.5	20.1	21.3
Or	81.4	94.9	91.8	92.8	96.1	93.6	94.4	0.5	0.6	0.5	0.5	0.8	1
Fe/Fe + Mg	–	–	–	–	–	–	–	–	–	–	–	–	–

Table 1. *(Continued.)*

Sample no.	JHG1/ TS15	JHG1/ TS15	JHG1/ TS15	JHG1/ TS15	JHG1/ TS15	JHG1/ TS15	JHG1/ TS15	JHG1/ TS15	JHG1/ TS15	JHG1/ TS15	JHG1/ TS15	JHG1/ TS15	JHG1/ TS15
Mineral	Plag	Plag	Plag	Plag	Bt	Bt	Bt	Bt	Bt	Bt	Bt	Bt	Bt
Analysis	6/1	8/1	4/1	5/1	15/1	16/1	17/1	18/1	19/1	20/1	23/1	24/1	5/1
Location	gmass	gmass	core	core	Jhiri	Jhiri	Jhiri	Jhiri	Jhiri	Jhiri	Jhiri	Jhiri	Jhiri
SiO_2	63.16	63.01	63.65	63.49	34.91	34.9	35.31	35.1	35.8	35.85	35.04	34.71	33.56
TiO_2	0.01	0.18	0	0	2.67	2.36	2.35	2.42	2.37	2.36	2.48	2.49	2
Al_2O_3	22.64	23.27	22.18	22.86	16.06	15.56	15.8	16.37	15.55	15.7	15.84	15.79	15.73
Cr_2O_3	–	–	–	–	0.17	0.15	0.2	0.03	0.03	0.13	0.09	0.15	0.66
FeO	0.08	0.31	0.07	0	22.18	23	23.18	21.95	22.09	22.63	23.36	21.86	21.08
MnO	0.06	0	0.04	0.05	0.16	0.14	0.11	0.29	0.13	0.19	0.24	0.21	0.21
MgO	0	0	0	0	7.55	7.57	7.76	7.78	8.04	8.14	7.92	7.86	7.55
CaO	4.23	4.12	3.54	4.01	0.04	0.05	0.08	–0.02	0.02	0.1	–0.01	0.02	0.17
Na_2O	8.96	9.03	9.54	9.49	0.14	0.11	0.11	0.08	0.07	0.07	0.05	0.1	0.46
K_2O	0.11	0.19	0.1	0.06	9.39	9.37	9.04	9.82	9.32	9.61	9.62	9.17	8.68
Sum	99.25	100.11	99.12	99.96	93.27	93.21	93.94	93.82	93.42	94.78	94.63	92.36	90.1
Oxygen	32	32	32	32	22	22	22	22	22	22	22	22	22
Si	11.242	11.141	11.333	11.226	5.795	5.824	5.829	5.794	5.911	5.861	5.771	5.81	5.762
Al	4.746	4.845	4.651	4.76	2.205	2.176	2.171	2.206	2.089	2.139	2.229	2.19	2.238
Fe_3	0	0	0	0	0	0	0	0	0	0	0	0	0
Ti	0.001	0.024	0	0	0.333	0.296	0.292	0.3	0.294	0.29	0.307	0.314	0.258
Fe_2	0.012	0.046	0.01	0	3.079	3.21	3.2	3.03	3.05	3.094	3.218	3.06	3.027
Cr	–	–	–	–	0.022	0.02	0.026	0.004	0.004	0.017	0.012	0.02	0.089
Mn	0.009	0	0.006	0.007	0.022	0.02	0.015	0.041	0.018	0.026	0.033	0.03	0.031
Mg	0	0	0	0	1.869	1.883	1.91	1.914	1.979	1.984	1.945	1.961	1.933
Ca	0.807	0.78	0.675	0.76	0.007	0.009	0.014	−0.004	0.004	0.018	−0.002	0.004	0.031
Na	3.092	3.096	3.294	3.254	0.045	0.036	0.035	0.026	0.022	0.022	0.016	0.032	0.153
K	0.025	0.043	0.023	0.014	1.989	1.995	1.904	2.068	1.963	2.004	2.021	1.958	1.901
Sum	19.934	19.975	19.992	20.021	16.301	16.351	16.296	16.355	16.269	16.339	16.393	16.302	16.366
Ab	78.8	79	82.5	80.8	–	–	–	–	–	–	–	–	–
An	20.6	19.9	16.9	18.9	–	–	–	–	–	–	–	–	–
Or	0.6	1.1	0.6	0.3	–	–	–	–	–	–	–	–	–
Fe/Fe + Mg	–	–	–	–	0.62	0.63	0.63	0.61	0.61	0.61	0.62	0.61	0.61

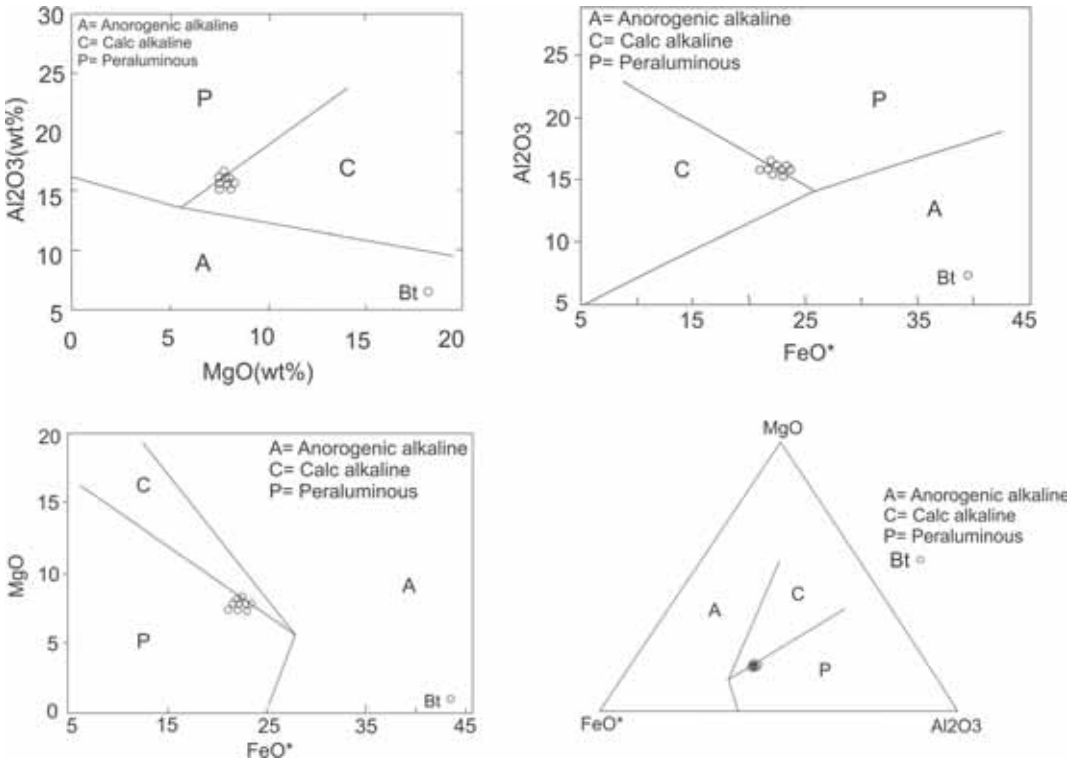

Figure 14. Biotite plot of Jhiri granite after Abdel-Rahman (1994). All the oxide data are in weight percentage and FeO as total Fe. The biotites plot in the boundary of Peraluminous and Calc-alkaline field.

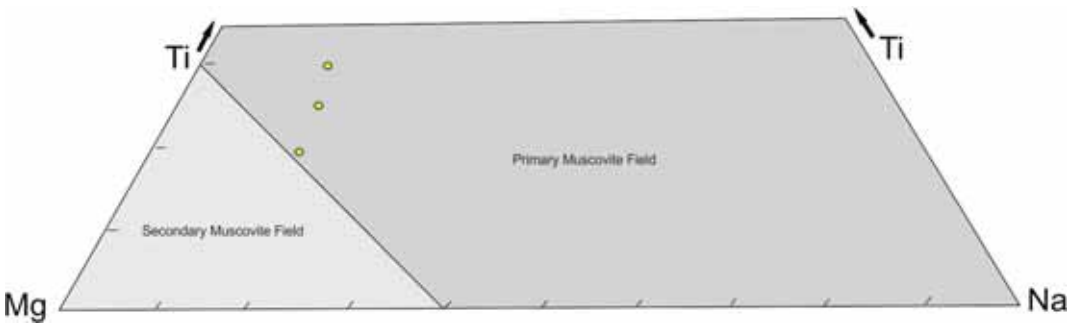

Figure 15. Plots of muscovite chemical composition data in Ti *vs.* Mg–Na diagram proposed by Miller *et al.* (1981) for discrimination of primary and secondary muscovite. The muscovites of Jhiri pluton fall in the primary field suggesting their magmatic origin.

values of major oxide have been plotted in the Total Alkali *vs.* Silica (TAS) diagram of Middlemost (1985) where out of six samples; four samples were plotted in the granite field, whereas the rest two samples were plotted in the quartz monzonite field (figure 16).

Frost *et al.* (2001) proposed several discrimination diagrams using different major oxide proportions for granitic suite of rocks. They proposed a three tier classification scheme namely Fe* [Total FeO/(Total FeO + MgO)], Modified Alkali Lime Index (MALI) and Alumina Saturation Index (ASI). The study suggested that the change of these three factors can be linked to differentiation history of granitic magma, composition and abundances of the feldspars in the rock which is again related to magma source and also the composition of minor minerals which is dependent on magma sources and conditions of melting. In order to test the alumina saturation of the pluton, Alumina Saturation Index (ASI) of Frost *et al.* (2001) were calculated and ranges in between 0.94 to 1.23 with the molar Na and K is less than molar Al, i.e., Na+ K<Al suggesting the granite to be peraluminous to weakly meta-aluminous in character (figure 17). The MALI index as proposed by Frost

Table 2. *Whole rock analytical data of Jhiri granite; the values have been normalized with respect to chondrite composition after Nakamura (1974).*

Sample no.	JHG/PCS-1	JHG/PCS-2	JHG/PCS-4	JHG/PCS-5	JHG/PCS-7	JHG/PCS-8
Latitude	27.2196102	27.2224903	27.2262497	27.2211056	27.2224808	27.227272
Longitude	76.2187805	76.2179947	76.2144165	76.2163391	76.2153778	76.2119293
SiO_2	63.9	63.32	65.09	65.45	66.1	66.54
TiO_2	1.16	1.11	0.83	0.05	1.0	0.81
Al_2O_3	14.33	14.85	14.28	15.32	13.46	13.53
$Fe_2O_3^T$	5.18	6.5	5.68	6.48	6.11	4.97
CaO	1.83	1.87	1.24	1.84	1.83	1.48
MgO	2.72	2.09	1.55	0.93	1.49	1.24
Na_2O	5.87	3.53	2.08	7.41	4.12	3.95
K_2O	2.33	4.88	5.99	0.77	3.19	4.21
MnO	0.02	0.06	0.04	0.05	0.05	0.04
P_2O_5	0.62	0.59	0.50	0.06	0.56	0.45
LOI	1.88	1.22	1.75	1.71	1.92	1.96
Total	99.84	100.02	99.03	100.07	99.83	99.18
Ba	295	598	594	< 5	340	440
Ga	62	47	42	9	36	26
Sc	11	13	6	29	8	7
V	74	75	53	69	73	57
Th	40	90	44	65	60	18
Pb	80	128	111	19	54	53
Ni	16	14	15	48	21	20
Co	34	36	34	42	11	13
Rb	195	300	312	44	263	240
Cr	37	18	8	17	33	23
Sr	150	187	151	112	132	159
Zr	443	379	350	13	433	328
Nb	46	49	37	23	40	29
Cu	18	18	12	235	34	17
Zn	161	263	209	245	104	98
Be	2.67	2.12	2.22	1.18	2.04	2.25
Ge	0.76	0.84	0.79	0.55	0.92	0.81
Y	25.2	23.2	23.01	9.64	39.7	28.73
Mo	1.57	1.16	0.59	2.45	<0.50	<0.50
Sn	1.75	1.29	<1	<1	1.56	1.21
La	48.53	90.66	77.09	49.78	87.7	31.39
Ce	106.98	194.8	130.05	115.49	186	67.95
Pr	10.87	21.3	16.5	11.07	20.8	9.38
Nd	44.78	81.06	65.08	41.25	78.7	40.34
Sm	9.23	12.45	9.98	6.66	13	9.22
Eu	1.84	1.22	1.35	1.11	1.19	1.27
Gd	6.92	9	7.48	4.74	10.4	7.77
Tb	1.01	1.16	1.02	0.57	1.57	1.19
Dy	4.62	4.57	4.32	2.08	7.49	5.64
Ho	0.94	0.85	0.84	0.38	1.46	1.08
Er	2.54	2.35	2.28	1	4.07	3.00
Tm	0.33	0.31	0.33	0.14	0.6	0.39
Yb	2.08	1.89	1.75	0.9	3.92	2.16
Lu	0.27	0.26	0.25	0.13	0.56	0.25
Hf	11.26	9.85	12.54	6.69	16.3	12.61
Ta	1.44	1.94	1.56	1.74	3.55	1.75
U	4.09	4.98	4.08	7.53	7.22	4.70

Table 2. *(Continued.).*

Sample no.	JHG/PCS-1	JHG/PCS-2	JHG/PCS-4	JHG/PCS-5	JHG/PCS-7	JHG/PCS-8
∑REE	240.94	421.88	318.32	235.3	417.47	181.08
$(La/Yb)_N$	15.55	31.98	29.37	36.87	14.92	9.66
$(La/Sm)_N$	3.23	4.48	4.75	4.6	4.16	2.09
$(Gd/Yb)_N$	2.65	3.79	3.40	4.19	2.10	2.85
Eu/Eu*	0.71	0.35	0.48	0.61	0.32	0.46
A/CNK	0.92	1.03	1.17	0.94	0.99	0.98
10000 ∗ Ga/Al	4.23	3.12	2.86	0.57	2.61	1.86
T_{Zr}°C (Miller *et al.* 2003)	897	889	900	616	904	878
T_{Zr}°C (Watson and Harrison 1983)	848	848	863	587	864	837
CIPW norm						
Q	14.92	18.89	27.19	15.04	25.89	24.38
C	0.31	1.80	3.39	0	1.25	0.88
Or	14.05	29.19	36.39	4.59	19.27	25.59
Ab	50.70	30.20	18.13	63.75	35.62	34.37
An	5.13	5.48	2.99	6.38	5.55	4.52
Di	0	0	0	1.92	0	0
Hy	6.91	5.27	3.97	1.45	3.77	3.17
Mt	0	0	0	0.01	0	0
Il	0.04	0.13	0.09	0.09	0.11	0.08
Hm	5.28	6.59	5.84	6.57	6.24	5.11
Ru	1.16	1.03	0.80	0	0.96	0.78
Ap	1.49	1.42	1.21	0.14	1.34	1.09

Raw point count data (Modal)

Sample no.	Counts	Quartz (Q)	Alkali feldspar (A)	Plagioclase feldspar (P)	Biotite (Bt)	Muscovite (Mus)	Accessory (Acc)	Q%	A%	P%
JHG/TS-1	300	67	171	40	8	10	4	24.1	63.35	12.55
JHG/TS-2	300	37	138	66	39	20	0	15.32	57.28	27.4
JHG/TS-3	300	72	137	34	51	3	3	29.66	56.37	13.97
JHG/TS-4	300	87	122	44	28	17	2	34.44	48.22	17.34

et al. (2001) has been calculated and plots show the pluton falls in the alkali-calcic and near to the transition line of alkalic fields (figure 18). The Fe number (Fe*), ratio of total FeO/total FeO + MgO as proposed by Frost *et al.* (2001) has also been plotted where most samples plot within magnesian field, near to the ferroan-magnesian boundary, but within the broad field of A-type granites as demarcated in their study except one sample which lies outside the field (figure 19). Thus synthesis of major oxide chemistry shows Jhiri granite to be peraluminous to weakly meta-aluminous, magnesian to slightly ferroan, A-type pluton. Moreover, the major oxide chemistry of the Jhiri granite shows resemblance with the high-K, alkali-calcic post-tectonic Caledonian granitoids which have been demonstrated as post-orogenic granitoids (Maniar and Piccoli 1989), shoshonitic granitoids (Duchesne *et al.* 1998).

4.3.2.2 *Trace and REE chemistry:* The trace elements chemistry of the pluton shows moderate values of Ba (295–598 ppm), Rb (195–312 ppm) and Sr (132–187 ppm) except the sample no. JHG/PCS-5 which shows an altogether different concentration. Such an abnormality can be interpreted as the effect of later metasomatism as postulated in the study carried out by Kaur *et al.* (2017) in parts of the NDT. The trace and REE elemental concentration are often normalized and are plotted in multi-element spider diagram to study the different geochemical patterns. The primitive mantle normalised multi-element spider plot of Jhiri granite after McDonough and Sun (1995) shows a strong negative anomaly for large ion lithofile elements (LILE) like Ba, Sr along with P and high field strength elements (HFSE) like Ti, whereas strong positive anomaly of Pb, Nd and Th (figure 20). The chondrite normalised REE plot of the samples after

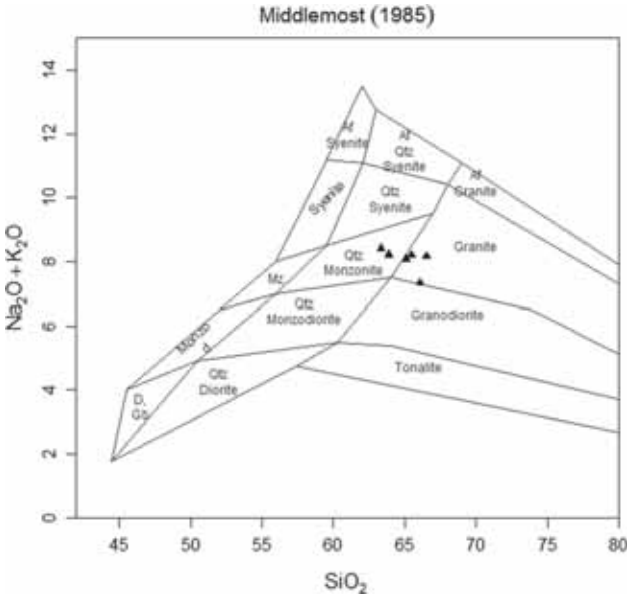

Figure 16. Total Alkali *vs.* Silica diagram after Middlemost (1985) for Jhiri granite. Out of six samples, four samples plot in granite field and two samples plot in Qtz Monzonite field.

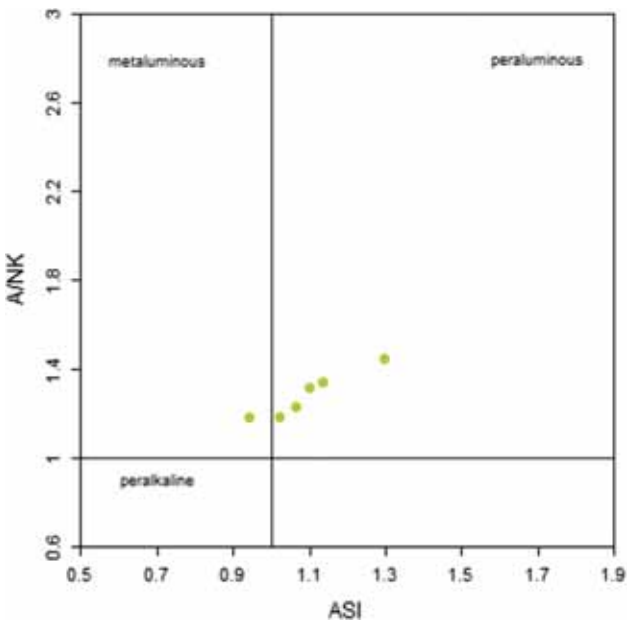

Figure 17. A/NK *vs.* ASI diagram after Frost *et al.* (2001). Plots show that most of the samples of the pluton fall in the peraluminous field whereas one sample plots in the metaluminous field of Frost *et al.* (2001).

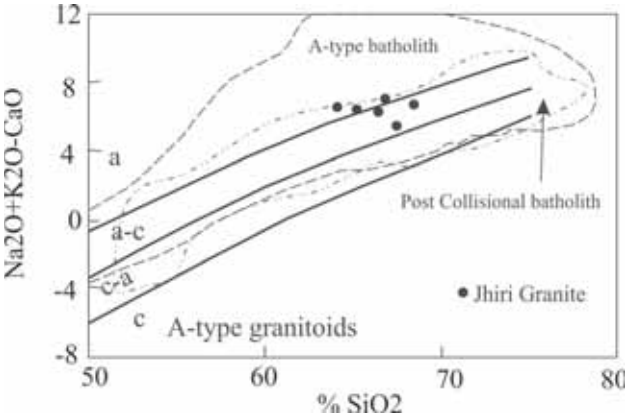

Figure 18. $Na_2O + K_2O - CaO$ *vs.* SiO_2 diagram (MALI index) after Frost *et al.* (2001). Plots show that the pluton falls in the Alkali-Calcic and near to the transition line of Alkalic fields; dash-dot line represents fields of Caledonian Granitoids whereas dashed line represents the overall A-type field, from Frost *et al.* (2001).

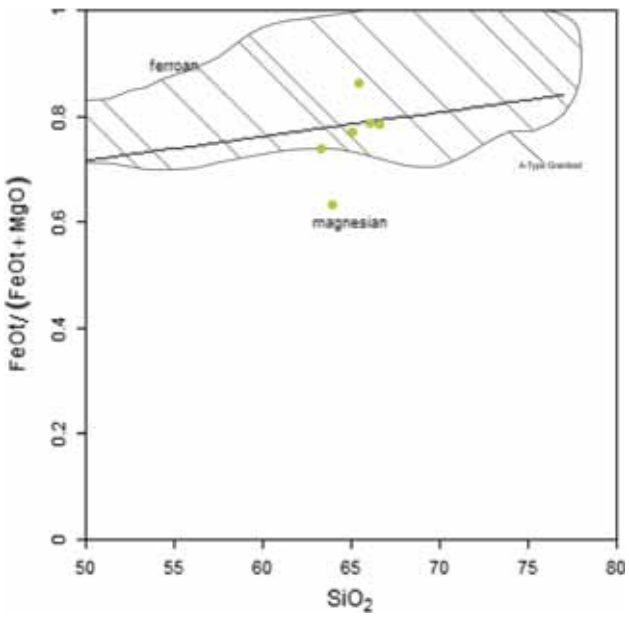

Figure 19. $FeO_t/(FeO_t + MgO)$ *vs.* SiO_2 plot of Jhiri granite (after Frost *et al.* 2001), most of the samples are plotted in magnesian field, near to the ferroan-magnesian boundary, fields are from Frost *et al.* (2001).

Nakamura (1974) show an enriched L-REE pattern with a strong depletion in H-REEs and moderately negative Eu anomaly (figure 21). The multi-element REE plot and chondrite normalised REE abundance profiles exhibit moderate fractionation pattern. The $(La/Yb)_N$ value of the samples vary from 9.66 to a maximum of 36.87 (table 2). The REE plots also show moderately negative Eu anomalies with Eu/Eu* values ranging from 0.32 to 0.71 (table 2). The LREE plot show a moderate enrichment pattern with $(La/Sm)_N$ values ranging from 2.09 to 4.75. The HREEs show a strong depletion pattern with $(Gd/Yb)_N$ values ranging from 2.10 to 4.19 (table 2). Moreover, the pluton is characterised by strong negative peaks for Sr, Ti and P and relatively less prominent Eu anomaly. The strongly depleted HREE pattern suggests

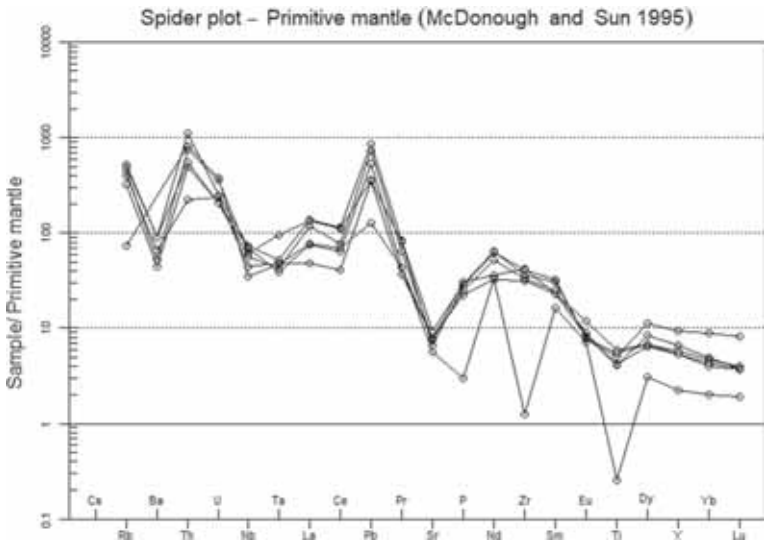

Figure 20. Multi-elemental spider plots for Jhiri granite after McDonough and Sun (1995).

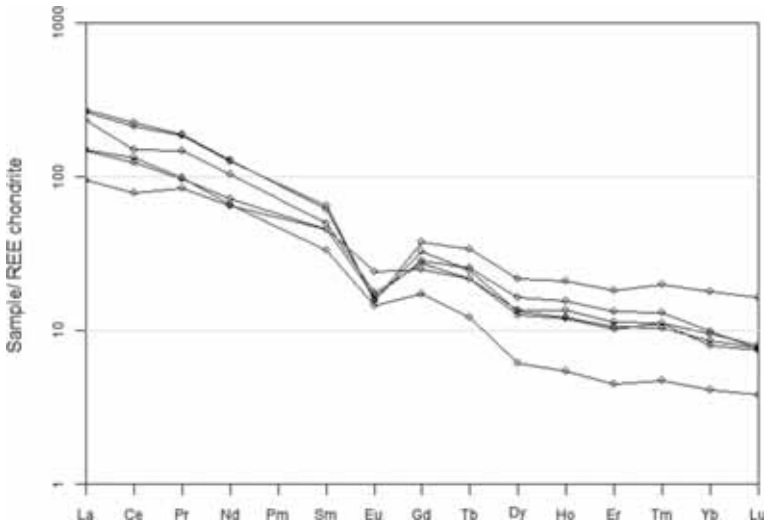

Figure 21. Chondrite normalised REE plot of Jhiri granite after Nakamura (1974).

generation of the melt from a garnet and hornblende free source. The moderate Eu anomaly can be explained with lesser differentiation history of the melt, whereas the negative peaks for Sr and P are linked with greater fractionation of plagioclase and apatite, respectively. The Ti depletion of the rock can be interpreted due to fractionation of ilmenite in the system.

Collins *et al.* (1982), Whalen *et al.* (1987), and Sylvester (1989) have proposed several discrimination diagrams using different trace element chemistry for identification of A-type granitoids and also to denote their possible tectonic settings. Collins *et al.* (1982) suggested higher Ga/Al ratios as an important criterion in identifying A-type plutons. Using this analogy, Whalen *et al.* (1987) proposed a number of A-type granitoid discriminantion diagrams. The plots of Jhiri granite in the discrimination diagrams proposed by Whalen *et al.* (1987) lie in the A-type field (figure 22) except one sample (JHG/PCS-5). In order to further classify the A-type granites, Eby (1992) suggested that A-type granites can be chemically divided into two groups, the A_1 group and the A_2 group. The A_1 group of rocks, he opined are mantle differentiates which generally got contaminated to a greater or lesser extent by continental crust whereas the A_2 group of rocks show affinity towards average continental margin and island arc basalts. The A_1–A_2 plot as proposed by Eby (1992) of Jhiri granite shows all sample plots in the A_1 field (figure 23) suggesting possible magma generation in extension settings.

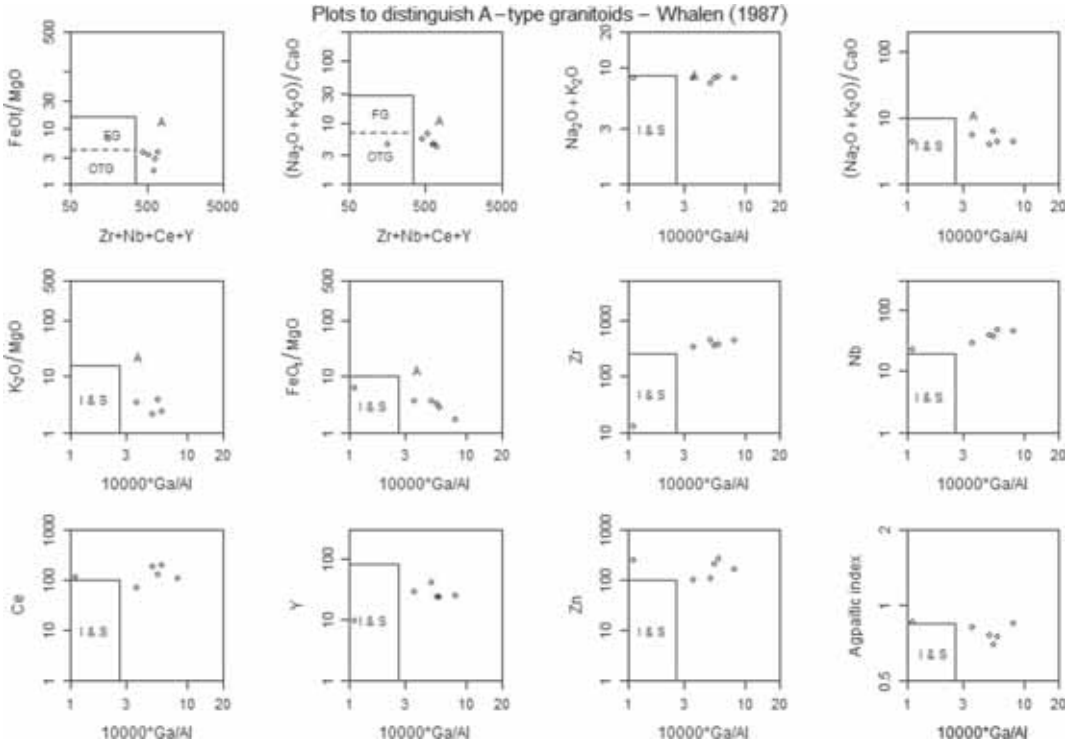

Figure 22. Plot of Jhiri pluton in the discrimination diagram proposed by Whalen *et al.* (1987) for A-type granitoids. All samples of Jhiri granite plot in the A-type granite field.

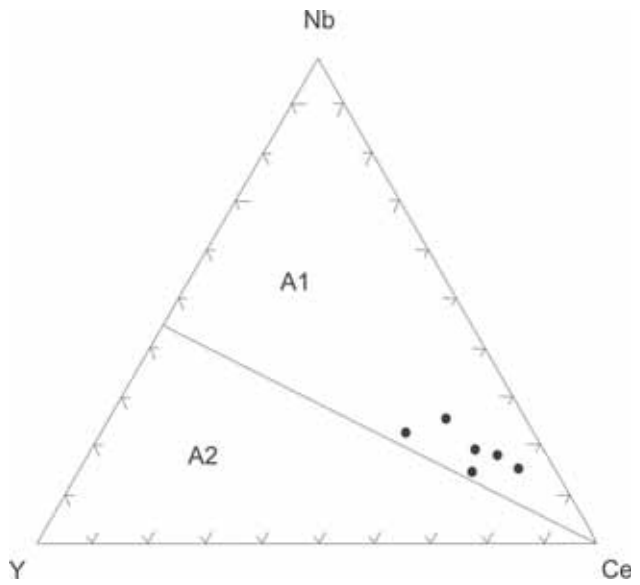

Figure 23. Sample plot of Jhiri granite pluton on the A_1–A_2 plot of Eby (1992); all samples of Jhiri granite plot in the A_1 field.

4.4 *Geochronology*

The morphology of the separated zircon grains was studied with the help of back scattered electron (BSE) and cathode luminescence (CL) images (figure 8). The studied zircons show a wide variety in their morphology. Overall the zircon crystals can be subdivided into two broad groups, the zircons showing zoning in the internal structure and the zircons crystals devoid of any zoning. The zoned zircons often show presence of overgrowth surrounding the earlier boundaries suggesting major thermal event at later periods. Some of the zoned zircons show presence of oscillatory zoning which clearly indicate their magmatic origin. The size of the zircon crystal varies from 400 to 200 μm (figure 24).

Twentyfive spot analyses from 18 zircons were carried out. The results of the sample along with zircon standards 91500 (primary) and Plesovice (secondary) are given in table 3. Data thus obtained has been presented through Wetherill's U–Pb Concordia plots using Isoplot 4.05 data regression software tool (Ludwig 2012). The ages are represented by weighted mean as it is the statistical model most often applied to a set of individual analyses and the result is often interpreted as the best estimate of the age of a sample (Schoene 2014). Zircon standard 91500 was used as primary reference material for calibration during experiment. Concordia plots (Wetherill 1956) and calculation of weighted mean age were carried out using IsoplotR (Vermeesch 2018). Plešovice Zircon $^{206}Pb/^{238}U$ with age of 337.13 ± 0.37 Ma (ID-TIMS) reported by Sláma *et al.* (2008) was used as

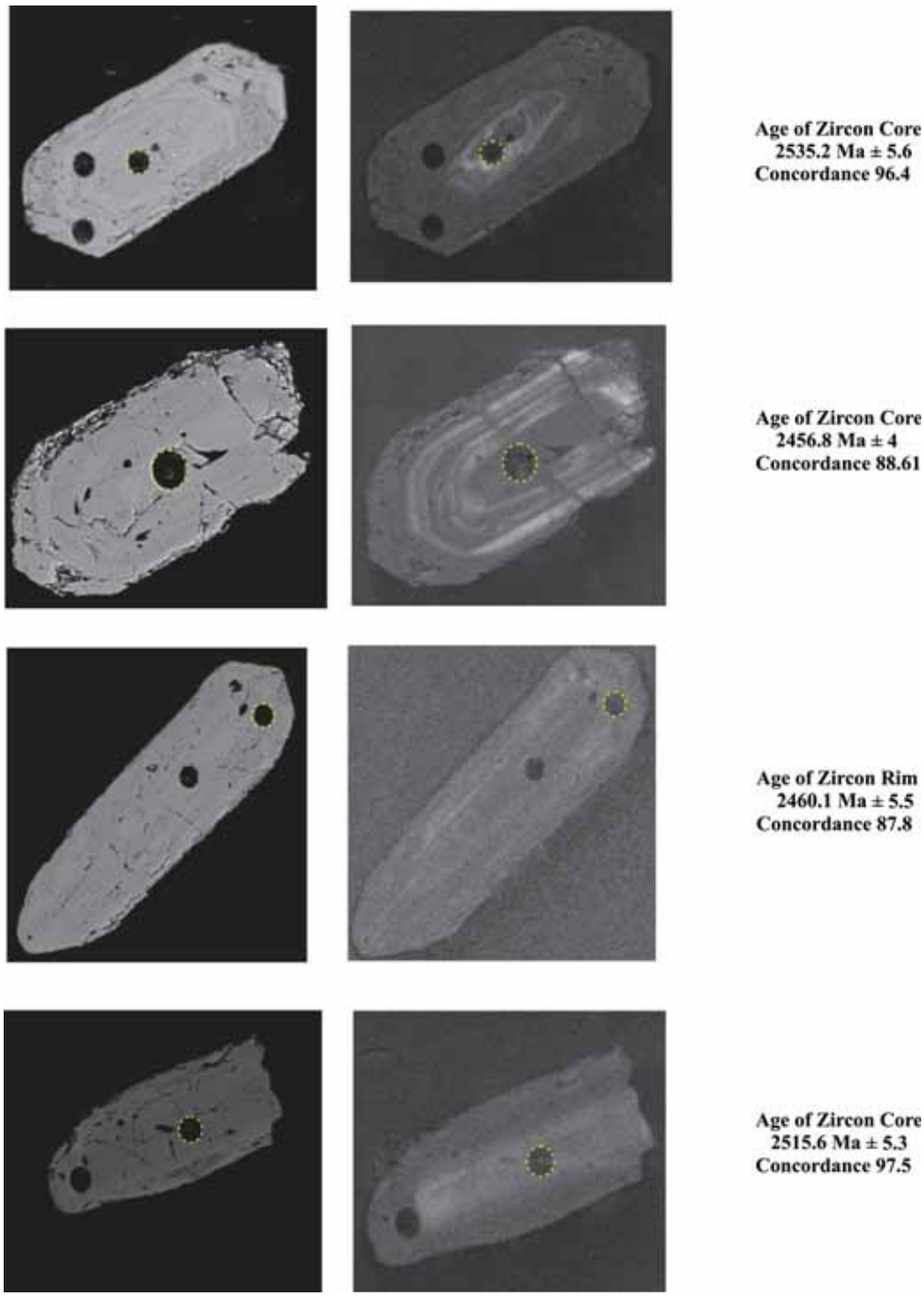

Figure 24. Back Scatter Electron (BSE) and Cathod Luminescence (CL) of representative zircon crystals of Jhiri granite showing internal structure of the analyzed zircons along with laser ablazed spots; the absolute age of the zircons are also mentioned along with the concordance.

secondary standard zircon. During analysis the weighted mean $^{206}Pb/^{238}U$ age of 335.40 ± 6.60 Ma ($n = 4$, MSWD = 1.7) was obtained for this Plešovice Zircon. The analysis of 18 zircons from granite sample show more or less consistent $^{207}Pb/^{206}Pb$ ages and yielded a weighted mean $^{207}Pb/^{206}Pb$ age of 2466 ± 39 Ma (figure 25). In the $^{206}Pb/^{238}U$–$^{207}Pb/^{235}U$ Concordia diagram (figure 25) few plots deviate from the Concordia and has been interpreted as Pb loss possibly due to a later thermal event (probably 1700–1800 Ma). The Rho values range in between 0.98 and 1, whereas the concordance value ranges from 60% to about 102%. Higher concordance value has been received for 14 analyses points out of the total 25 with a concordance value >90%.

Table 3. *Zircon U–Pb isotopic data of Jhiri granite.*

Jhiri granite sample	$^{207}Pb/^{235}U$	2σ	$^{206}Pb/^{238}U$	2σ	Error-correlation/ Rho values	$^{207}Pb/^{235}U$	2σ	$^{206}Pb/^{238}U$	2σ	$^{207}Pb/^{206}Pb$	2σ	Concordance	U ppm	Error	Th ppm	Error	Pb ppm	Error
5 core	10.03	0.18	0.4321	0.0075	0.98	2432	16	2311	34	2540.5	5.1	90.97	728	15	400.8	6.9	79	16
6 core	10.65	0.23	0.4678	0.0095	0.99	2486	20	2470	41	2523.4	7.7	97.88	271	12	270	15	245	18
8 core	10.42	0.25	0.458	0.011	0.99	2461	23	2420	47	2517.5	4.5	96.13	168.7	6.7	256.7	8.6	291	10
9 rim	8.77	0.23	0.4	0.01	1.00	2303	25	2160	48	2460.1	5.5	87.80	434.7	7.6	508	15	135.6	5.3
12 core	10.62	0.25	0.463	0.11	0.98	2485	22	2444	47	2535.2	5.6	96.40	285.2	6.1	122.6	2.2	172.4	7.2
13 core	10.47	0.24	0.461	0.01	0.99	2485	21	2454	46	2515.6	5.3	97.55	66.1	1.6	47.4	1.1	38.2	2.6
14 core	11.08	0.21	0.4783	0.0088	1.00	2525	18	2520	39	2538	2.9	99.29	389.9	7	309.1	3	316.9	4.3
15 core	10.91	0.29	0.469	0.013	0.99	2509	25	2476	55	2546.5	4	97.23	74.1	1.8	55.1	2.7	48.2	1.6
15 rim	10.88	0.23	0.4707	0.0097	1.00	2502	21	2479	43	2531.8	3.9	97.91	470	11	250	10	152	3.6
16 core	8.89	0.18	0.4022	0.0079	0.99	2322	19	2177	36	2456.8	4	88.61	270.4	5.4	275	13	95.3	1.6
18 core	7.47	0.16	0.3183	0.0068	0.99	2159	20	1777	33	2556.5	3.9	69.51	263.9	8.3	763	18	256.5	4.6
20 core	10.02	0.26	0.469	0.012	1.00	2433	24	2475	51	2419	5	102.32	465.6	5.9	428	10	293.4	4.1
22 core	9.21	0.24	0.4082	0.0096	0.99	2349	23	2204	44	2483.8	6.1	88.74	466.4	6.8	186.5	8.7	34.1	1.3
24 core	9.39	0.29	0.402	0.013	0.99	2364	29	2168	58	2539.7	4.6	85.36	99.8	3.3	466	10	133.6	4.8
24 rim	9.19	0.3	0.415	0.013	1.00	2350	29	2226	60	2454.7	3.5	90.68	286.9	5.8	533	12	201.8	3.9
26 core	9.49	0.25	0.417	0.011	1.00	2379	24	2247	48	2496.3	3.2	90.01	231.6	9.9	261.6	5.5	103.2	3.7
27 core	10.83	0.32	0.47	0.014	1.00	2503	28	2490	60	2515.4	3.2	98.99	148.4	2.7	257.6	4.7	243	3.9
27 rim	9.97	0.22	0.451	0.01	0.99	2427	21	2399	45	2449.6	3.4	97.93	266.1	3.9	83	1.1	90.1	1.8
28 core	5.04	0.14	0.223	0.0062	0.99	1821	24	1300	33	2489.6	4.6	52.22	101.2	2.3	102	1.7	56	1.5
28 core	6.12	0.15	0.3126	0.0075	1.00	1991	22	1753	37	2245.3	3.5	78.07	498	15	299.4	9.5	160.4	3.1
29 core	9.08	0.18	0.3835	0.0074	0.99	2341	18	2089	35	2569.4	3.2	81.30	166.2	4.7	212.3	6.2	173	4.2
29 inter	6.01	0.13	0.3217	0.0064	0.99	1973	19	1798	31	2160.9	5.7	83.21	568	19	272	12	223.1	9.3
29 rim	4.64	0.073	0.2351	0.0036	0.99	1754	13	1360	19	2258.8	3.8	60.21	725	12	121.8	1.3	216.9	2.4
35 core	10.36	0.24	0.457	0.01	0.99	2461	21	2421	45	2495.9	2.8	97.00	242.5	3.2	50.97	0.72	56.6	1.4
35 rim	10.05	0.22	0.468	0.01	0.98	2437	20	2470	44	2403.7	6.8	102.76	135.1	2.6	52.25	0.73	67.5	2.5

Table 3. *(Continued.)*

Jhiri granite sample	$^{207}Pb/^{235}U$	2σ	$^{206}Pb/^{238}U$	2σ	Error-correlation/ Rho values	$^{207}Pb/^{235}U$	2σ	$^{206}Pb/^{238}U$	2σ	$^{207}Pb/^{206}Pb$	2σ	Concordance	U ppm	Error	Th ppm	Error	Pb ppm	Error
91500 Zircon (Primary standard)																		
1	1.85	0.038	0.1792	0.0035	0.95712	1061	14	1065	19	1064	12	100.09	79.8	1.4	29.97	0.45	15	2.3
2	1.852	0.032	0.1791	0.0029	0.96594	1066	12	1063	16	1063.8	9.1	99.92	80.2	1.3	30.05	0.4	15	1.2
3	1.85	0.026	0.1792	0.0022	0.96073	1062.1	9.4	1064	13	1063.8	9.5	100.02	80	1.1	30	0.32	15	0.96
4	1.871	0.037	0.1796	0.0034	0.96562	1067	13	1064	19	1071	9.4	99.35	79.11	0.99	29.72	0.34	14.81	0.93
5	1.885	0.029	0.1781	0.0026	0.9568	1055	11	1056	14	1056	11	100.00	81.5	1	30.53	0.35	15.1	1
6	1.856	0.025	0.18	0.0021	0.95122	1064.6	8.9	1059	12	1057.2	9.3	100.17	79.9	1.1	29.87	0.33	15.48	0.96
7	1.851	0.02	0.1789	0.0018	0.9301	1063.1	7.4	1060.8	9.9	1072.3	9.1	98.93	79.6	1	29.93	0.33	14.6	1.1
8	1.854	0.039	0.1786	0.0036	0.96807	1060	14	1059	19	1070	9.9	98.97	80.02	0.97	30.03	0.36	15.1	1.2
9	1.854	0.02	0.1793	0.0018	0.90129	1064.3	7	1063.7	9.7	1071.1	9.3	99.31	79.99	0.87	29.94	0.33	14.7	1.2
10	1.83	0.048	0.1797	0.0045	0.98268	1055	17	1063	25	1052.1	8.9	101.04	79.8	1.1	30.05	0.4	15.2	1.1
11	1.847	0.039	0.1793	0.0037	0.97596	1062	14	1063	20	1072.9	9.1	99.08	80.2	1.1	30.03	0.39	15.1	1.1
12	1.813	0.044	0.1773	0.004	0.97506	1049	16	1050	22	1052	10	99.81	79.9	1.1	29.99	0.4	14.9	1.2
13	1.863	0.036	0.1803	0.0033	0.97554	1066	13	1068	18	1067.5	8.6	100.05	79.91	0.99	29.96	0.36	15	1.1
14	1.855	0.051	0.1787	0.0049	0.98005	1062	18	1062	27	1068.1	9.8	99.43	80.1	1.1	30.07	0.47	14.9	1.3
15	1.854	0.032	0.1791	0.003	0.9703	1064	11	1063	16	1065	9.3	99.81	79.97	0.86	29.99	0.33	15	1.2
Plesovice Zircon (secondary standard)																		
1	0.429	0.014	0.0566	0.0017	0.96334	363.2	9.6	355	11	422	18		974	18	118.8	2.2	22	15
2	0.38	0.014	0.0525	0.0018	0.99326	327	10	329	11	336.4	9		707	12	82.1	1.5	12	1.8
3	0.388	0.015	0.0524	0.002	0.99486	331	11	329	12	363.3	8.5		697	14	82.3	1.5	13.3	1.1
4	0.382	0.015	0.0514	0.002	0.99584	325	11	322	12	354.5	8.5		681	14	80.4	1.5	11.86	0.99
5	0.383	0.014	0.0518	0.0018	0.99494	329	10	326	11	351.5	7.8		760	14	90.2	1.5	13.04	0.97
6	0.384	0.015	0.0514	0.002	0.99435	329	11	322	13	376.9	8.9		714	14	79.5	1.5	12.3	1
7	0.385	0.015	0.0515	0.002	0.99459	329	11	324	12	378.1	8.9		706	14	79.6	1.6	13.4	1
8	0.388	0.014	0.0519	0.0019	0.99497	332	10	326	12	371.4	8.2		711	14	80	1.4	12.6	1
9	0.389	0.01	0.0526	0.0014	0.99314	332.9	7.4	330	8.3	355	7.4		827	12	83	1.1	13.5	1.2
10	0.391	0.012	0.0526	0.0016	0.99316	334	8.6	329.9	9.6	358.5	7.6		756	12	89.2	1.2	13.7	1.2
11	0.3892	0.0066	0.05293	0.00087	0.98356	333.7	4.8	332.3	5.4	356.1	7.7		731.4	8.8	79.87	0.87	13.2	1.1
12	0.379	0.016	0.0512	0.0021	0.99563	323	12	321	13	362.9	8		658	13	65.9	1.1	11.1	1.2
13	0.3901	0.0065	0.05304	0.00087	0.9845	334.3	4.8	333	5.3	349.5	7.5		711.8	8	77.17	0.77	13.7	1.1
14	0.385	0.015	0.0518	0.002	0.99508	329	11	325	12	366	8.1		699	12	74.6	1.2	12	1.1
15	0.3874	0.0083	0.0529	0.00011	0.98729	332.5	6.1	331.9	6.5	350.7	8.1		782	10	74.95	0.85	11.3	1.1
16	0.3923	0.0072	0.05322	0.00094	0.98304	335.9	5.2	334.1	5.8	344.7	8.1		708	8.1	70.74	0.78	9.4	1

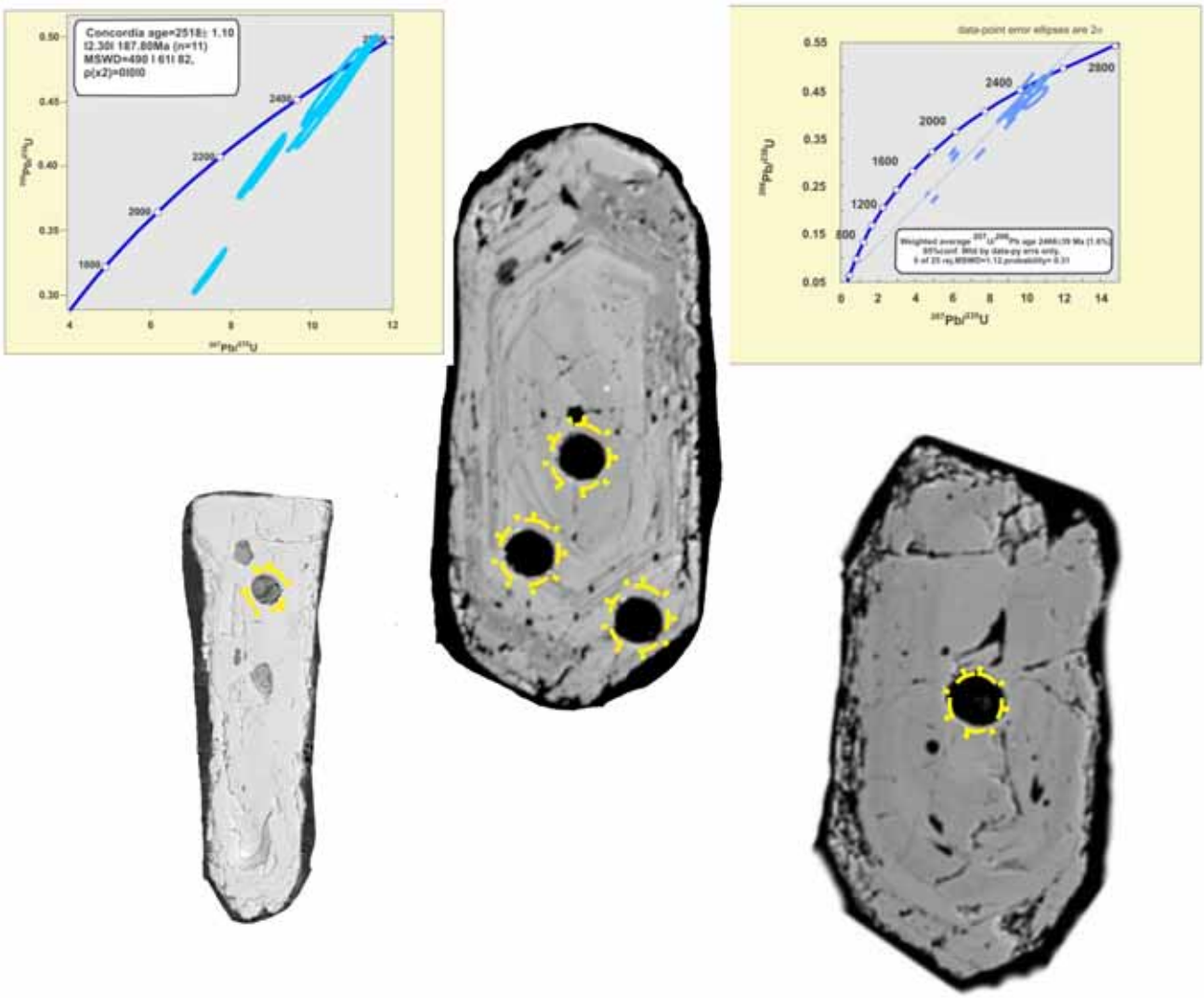

Figure 25. Back Scattered Image of selected zircons with analysis spots of Jhiri granite with the age Concordia. The Concordia diagram in the top right includes all analysis ($n = 25$) points with a Concordia age of 2466 ± 39 Ma, whereas the Concordia diagram in the top left represents part analytical data ($n = 11$) with a Concordia age of 2518 ± 1.1 Ma.

In order to achieve a more precise result 11 spot analysis from 10 zircons, with prominent zoning of magmatic nature have been used and yielded a concordia age of 2518 ± 1.1 Ma with MSWD of 490l61l82 (figure 25). The analyses show more or less consistent $^{207}Pb/^{206}Pb$ ages in a range of 2456–2556 Ma. The weighted mean of points with >95% concordance yielded age of 2529.60 ± 6 Ma (MSWD-6.8, $n = 7$) (figure 26). The age is interpreted as the crystallization age of Jhiri granite.

5. Discussion

5.1 *Petrogenesis*

The petrogenesis of granitoid pluton involves systematic study of the mineralogical and chemical characteristics for understanding the possible source rock of the magma generation, mechanisms of magma ascends and the tectonic settings in which the magma got emplaced in the earth's crust. The study of modal mineralogy and mineral chemistry data show the rock to be two mica granite with peraluminous character. The peraluminous nature is also reflected from the high ASI value of the studied biotites which suggest excess alumina in the magma after crystallisation of plagioclase which ultimately trapped by forming peraluminous minerals like biotite and muscovite. The feldspars chemistry of Jhiri granite shows similar composition of the plagioclase in the groundmass and in the phenocrystic core which indicate towards synchronous crystallization in the initial stage and afterwards shift of the crystallisation

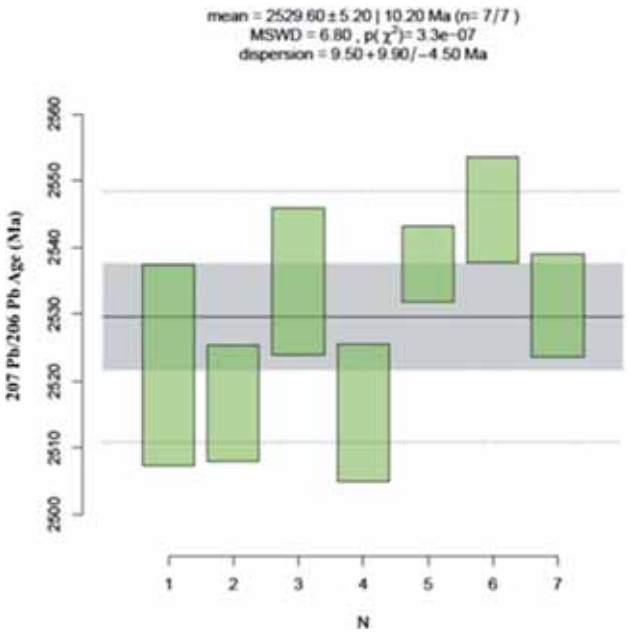

Figure 26. The weighted average $^{207}Pb/^{206}Pb$ zircon age of Jhiri granite. The crystallization age of the granite deduced in this study is 2529.6 ± 5.2 Ma ($n = 7$).

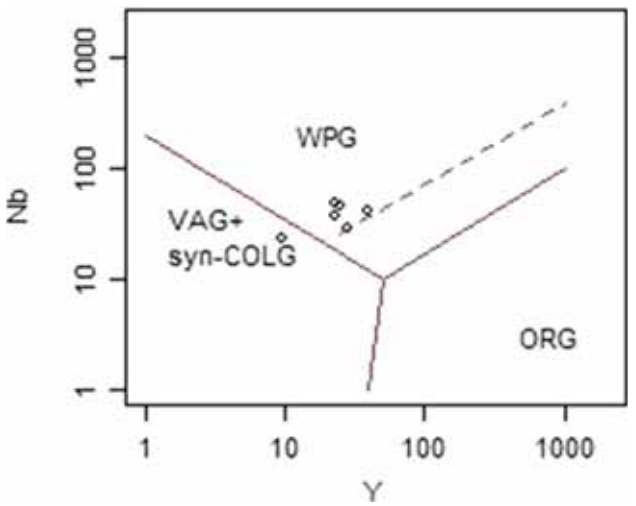

Figure 27. Tectonic discrimination diagram for Jhiri granite Nb *vs.* Y (after Pearce *et al.* 1984); WPG: within-plate granite; VAG: volcanic arc granite; syn-COLG: syn-collision granite; ORG: ocean ridge granite, most of the samples plotted in WPG field only one sample plotted in VAG + syn-COLG field.

front towards the alkali end. The change in the crystallization front from plagioclase to alkali can be interpreted in terms of a drop in P–T condition or increased fluidal activity in the system. The major oxide chemistry of the pluton reflects similar characteristics as is in case of mineral chemistry data with Fe* (Total FeO/Total FeO + MgO) value of 0.65–0.8 suggesting an enrichment of Fe in the magma composition compared to Mg. Moreover, the ASI value of Frost *et al.* (2001) ranges from 0.9 to a maximum of 1.2 which corroborates well with the idea of excess aluminium in the system during crystallization. The excess alumina and Fe as well as Mg can get accommodated in aluminous phases like biotite and muscovite.

Watson and Harrison (1983) proposed equations to determine the saturation temperature of zircon in case of fractional crystallization from magma which can be interpreted as the crystallization temperature of granite. The results show (table 2) T_{Zr} value of Jhiri samples varies from 836° to 863°C. The average of magma temperature as deduced from the equations is about 850°C. The value of one sample (JHG/PCS-5) deviates from this result due to abnormally low content of zirconium (Zr). Miller *et al.* (2003) proposed that solubility of zircon is extremely sensitive to temperature and suggested that zircon saturation thermometry (Watson and Harrison 1983) provides a simple and robust means of estimating magma temperatures. They provided an equation for determining T_{Zr} in zircon saturated magma and proposed two type of granites, 'cold granites' having $T_{Zr} \leq 800$°C and generally contain inherited zircon within and 'hot granites' $T_{Zr} \geq 800$°C and are devoid of any inherited zircon. The study proposed a possible collisional tectonics (thrusting) for origin of cold granites whereas the hot granites were interpreted as part of extensional or trans-tensional terranes. The value of T_{Zr} as calculated from the equation provided by Miller *et al.* (2003) of the Jhiri granite range between 878° and 899°C (table 2) with an average temperature of 890°C. Thus, the Jhiri granite can be classified as a 'hot granite, as per the classification proposed by Miller *et al.* (2003) and a temperature of 850°–890°C is proposed as the crystallization temperature of the granitoid.

The Jhiri granite bears similarities and dissimilarities with the known peraluminous granitoids reported across the globe. The peraluminous granitoids have been described as S-type (Chappel and White 1974), syn-collisional granitoids (Pearce *et al.* 1984), continental collisional granitoids (Maniar and Piccoli 1989) and muscovite peraluminous granites (Barbarin 1999). The general characteristics as described in these studies are that the rocks are muscovite bearing, high silica granitoids with absence of associated mafic rocks and in general have an Fe* number < 0.6. On the contrary, the Jhiri granite is less fractionated ($SiO_2 < 70\%$), small Eu/Eu* (0.32–0.71) value and

Table 4. *Instrument parameters of LA-MC-ICPMS.*

Laboratory and sample preparation	
Laboratory name	Geochronology and Isotope Geology Division, Geological Survey of India, Kolkata, India
Sample type/mineral	Igneous rocks
Sample preparation	Conventional mineral separation, 1 inch resin mount, Polish in 6, 3, 1 and 0.25 μ
Laser ablation system	
Make, Model and type	ESI/New Wave Research, NWR193
Ablation cell and volume	Standard large format cell
Laser wavelength (nm)	193 nm
Fluence (J cm^{-2})	5.6 J cm^{-2}
Repetition rate (Hz)	5 Hz
Ablation duration (s)	40 s
Aspect ratio of the size of spot	2:1 (35 μ/15 μ)
Sampling mode/pattern	Static spot ablation
Carrier gas	100% He in the cell, Ar make-up gas combined using a Y-piece 50% along the sample transport line to the torch
Cell carrier gas flow (l min^{-1})	0.2 l min^{-1}
ICP-MS Instrument	
Make, Model and type	Nu Instruments, Nu Plasma II MC-ICP-MS
Sample introduction	Ablation aerosol
RF power (W)	1300 W
Make-up gas flow (l min^{-1})	Aridus II DSN, 4.15 L/Min
Detection system	Mixed Faraday-multiple ion counting array
Masses measured	204–208, 235, 238
Gas blank	Masking syndrome by ^{204}Hg had been taken care by negligible $^{206}Pb/^{204}Pb$ ratio
Total integration time per output data point (s)	∼0.2 s (N.B. this should represent the time resolution of the data)
IC Dead time (ns)	14.7, 20.7, 24.9, 6.9 and 19.3 ns for IC0, IC1, IC2, IC3 and IC4, respectively
Mode of Data acquisition	Time Resolved Analysis (TRA) mode
Calibration strategy	91500 used as primary reference material, Plesovice as secondary/validation
Reference Material information	91500 (Wiendenbeck *et al.* 1995) Plesovice (Sláma *et al.* 2008)
Data processing package used/ Correction for LIEF	Iolite 2.5, U–Pb Geochronology3, DRS & IsoplotR for normalisation, uncertainty propagation and age calculation. LIEF correction assumes reference material and samples behave identically
Mass discrimination	Tl-tracer solution used for mass bias correction with $^{207}Pb/^{206}Pb$
Common-Pb correction, composition and uncertainty	No common-Pb correction applied to the data

shows an elevated Fe* (> 0.65). The granite shows similarity in geochemical characteristics with the Caledonian granitoids (Frost *et al.* 2001) with Fe* values lying in the magnesian field, alkali-calcic to alkali character and peraluminosity of the magma. The Caledonian granitoids have been described as post-orogenic granitoids (Maniar and Piccoli 1989) and K-rich calc-alkaline granitoids (Barbarin 1999) in earlier studies. In order to determine the possible tectonic setting of the granite magma generation, the analytical data were plotted in the Nb *vs.* Y discrimination diagrams proposed by Pearce *et al.* (1984) and the samples fall in the within plate granite (WPG) field, except one sample falling in the VAG field (figure 27). This data combined with the A_1–A_2 plot of Eby (1992) (figure 23) where all samples lie in the A_1 field with a much lower Y/Nb value (0.4–1; <1.2) suggest a mixed source of magma generation in case of Jhiri pluton. A mantle derived mafic melt mixing with shallow oxidised crustal melt is suggested. As per Forster *et al.* (1997), similar condition can arise where the source rock for the within plate granites were formed in an older volcanic arc.

5.2 *Comparison with other Neoarchean granitoids*

The northwestern part of the ADMB records existence of several Neoarchean granitoids such as

Table 5. *Whole rock analytical data of average Jhiri granite (this study), Berach Granite and Biotite Granite of Bundelkhand Craton; the data of Berach Granite and Biotite Granite are from Mondal and Raza (2013) and Kaur et al. (2016, 2019).*

Sample no.	Average Berach Granite (Mondal and Raza 2013)	Sample no. BR-1 (Berach Granite) (Kaur *et al.* 2019)	Average Jhiri granite	BK-2_Biotite granite (Bundelkhand) (Kaur *et al.* 2016)
SiO_2	65.10	66.70	65.07	75.3
TiO_2	0.53	0.33	0.83	0.15
Al_2O_3	15.19	15.05	14.30	13.31
Fe_2O_{3T}	4.75	3.35	5.82	1.4
CaO	2.04	2.28	1.68	0.57
MgO	2.39	2.18	1.67	0.44
Na_2O	4.14	3.30	4.49	3.21
K_2O	3.73	4.32	3.56	5.55
MnO	0.07	0.05	0.04	0.03
P_2O_5	0.18	0.15	0.46	0.04
Ba	863	853	377.83	435
Ga	17	18	37	–
Sc	9.2	–	12.33	–
V	57	48	66.83	15
Th	9.5	13.4	52.83	54.9
Pb	5.8	9	74.17	61
Ni	45	14	22.33	<20
Co	26	–	28.33	24
Rb	101	135	225.67	250
Cr	74	52	22.67	<20
Sr	224	299	148.5	98
Zr	106	140	324.33	121
Nb	13	8	37.33	14
Cu	32	–	55.67	–
Zn	75	51	180	50
Y	17	11	24.91	20
La	47	35.5	64.19	52
Ce	88	63.8	133.54	92.6
Pr	10	6.73	14.98	9.5
Nd	35	22.9	58.53	30.4
Sm	6.1	4.1	10.09	4.9
Eu	1.5	1.05	1.33	0.6
Gd	5.3	2.9	7.71	3.8
Tb	0.63	0.4	1.08	0.6
Dy	2.9	2.5	4.78	3.4
Ho	0.57	0.5	0.92	0.7
Er	1.5	1.4	2.54	1.9
Tm	0.22	0.23	0.35	0.3
Yb	1.4	1.6	2.11	2.5
Lu	0.22	0.23	0.28	0.4
Hf	2.5	3.6	11.54	4.3
Ta	2.9	–	1.99	2.2
U	2.1	2.7	5.43	13.3
$(La/Yb)_N$	22.84722	15.09983	20.63905	14.15556
Eu/Eu*	0.805064	0.929266	0.459924	0.424329

Gingla (2.6–2.4 Ga), Ahar River (2562 Ma), Untala (2505 Ma) and Berach (2540 Ma). All these plutons have been described as granodiorite, monzogranite, syenogranite to even quartz-monzogranite variety and classified as part of TTG suite, high-K granitoids or even Sanukitoids

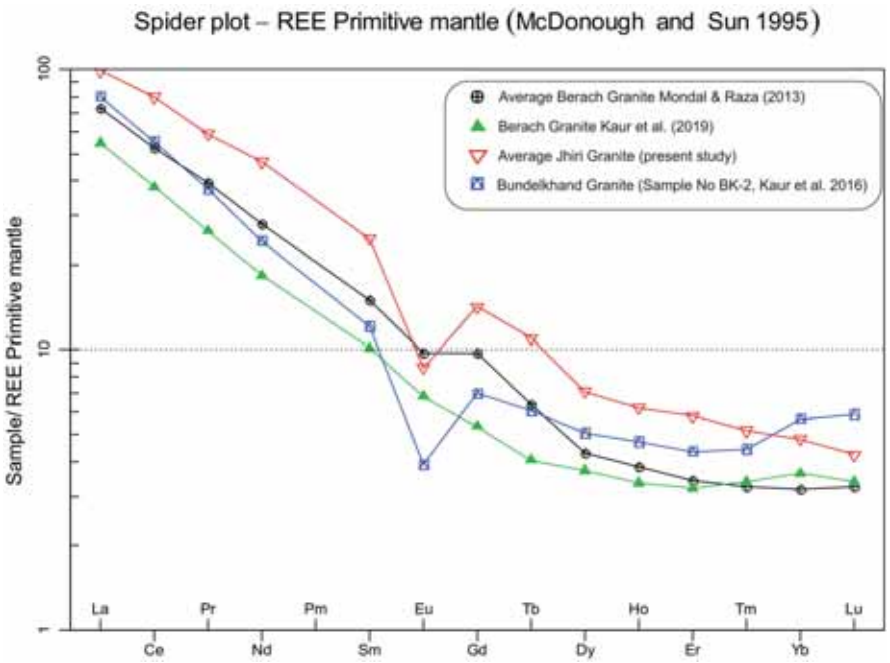

Figure 28. REE plot of average of representative samples of Jhiri granite ($n = 6$) with Berach granite (Mondal and Raza 2013, $n = 15$; Kaur *et al.* 2019, $n = 1$) and Biotite granite of Bundelkhand craton (sample no BK-2 of Kaur *et al.* 2016); the normalization values are after McDonough and Sun (1995).

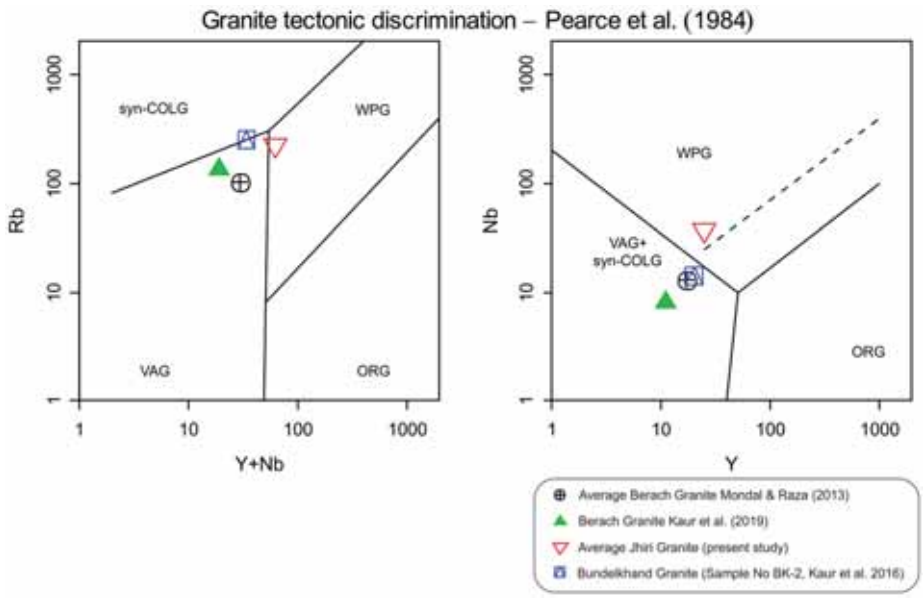

Figure 29. Tectonic discrimination diagram of Neoarchean granites; Rb *vs.* Y + Nb and Nb *vs.* Y (after Pearce *et al.* 1984); WPG: within-plate granite; VAG: volcanic arc granite; syn-COLG: syn-collision granite; ORG: ocean ridge granite; the Berach granite and Biotite granite of Bundelkhand craton falls in the VAG and syn-collisional granite field whereas Jhiri granite plots in the WPG field.

(Mondal and Raza 2013; Rahaman and Mondal 2014; Kaur *et al.* 2019). The rocks have been described either as intrusive bodies within basement TTG gneisses or as inliers surrounded by the older supracrustals (Aravalli Supergroup). The geochemical characteristics of these rocks have been described in detail by Rahaman and Mondal (2014). The general characteristics as reported in their study shows three broad groups such as TTG like, Sanukitoids and high-K granite. The plutons have a wide compositional range in terms of major and trace element chemistry with a moderately

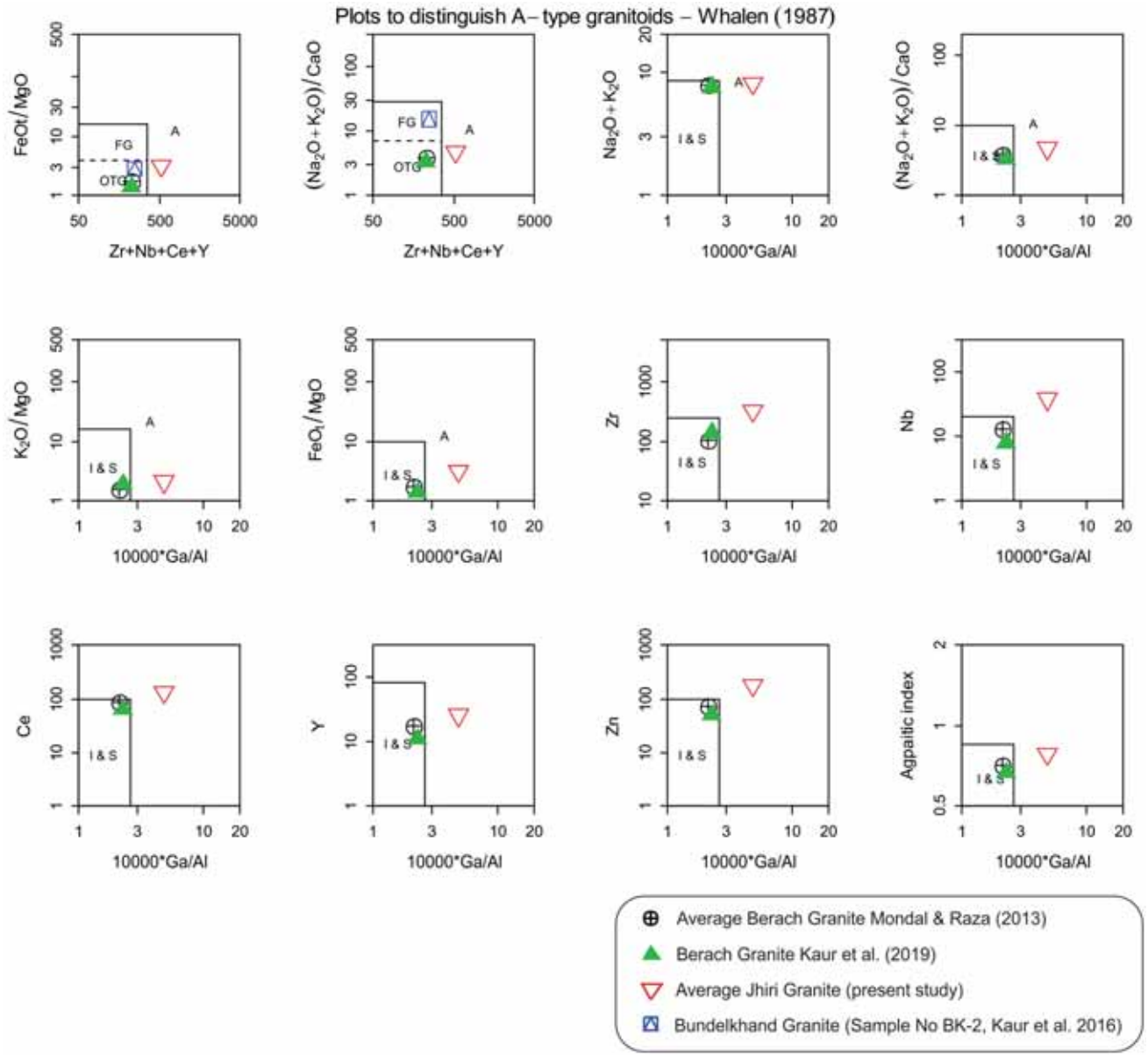

Figure 30. Tectonic discrimination diagram of Neoarchean granites (after Whalen *et al.* 1987); the Berach granite and Biotite granite of Bundelkhand craton falls in the I and S type granite field, whereas Jhiri granite plots in the A-type granite field.

close range (1.08–1.24) of A/CNK values for TTG like suites to a wide range of values (0.96–1.45) for the sanukitoids and high-K granite. The Shand's (1943) plot of these plutons show most of the sample plots in the peraluminous field except few samples of the sanukitoids group which plot in the meta-aluminous field. The peraluminosity of the plutons has been interpreted due to later alteration and release of K.

The results of Rahaman and Mondal (2014) on Neoarchean granitoids in the southern part of ADMB show overlapping geochemical characteristics in case of major element chemistry; thus discrimination between the three types of suites on the basis of major oxide chemistry is problematic. The trace and REE chemistry also show similar results with primordial mantle normalized moderate range of Eu/Eu* values for TTG and sanukitoids pluton (Eu/Eu* = 0.47–1.06) to an extreme range (Eu/Eu* = 0.33–4.78) for high-K granitoids. The $(Gd/Yb)_N$ values show a low to very high fractionation of HREE for TTG suite (1.12–5.71) and high-K granitoids (0.29–2.86) of rocks whereas a relatively close range (2.04–3.76) for the sanukitoids.

In comparison to other Neoarchean granitoids, the Jhiri granite shows a much closer range (1.4–1.53) of A/CNK value with slightly elevated

alumina content with respect to the sanukitoids. Similar characteristics is also observed in case of Eu/Eu*, where it ranges between 0.32 and 0.71 suggesting a distinct greater fractionation of plagioclase and a more evolved nature. In this context, the authors like to mention the study carried out by Mondal and Raza (2013) on Berach granite where they have carried out detailed geochemistry of the pluton and reported an ultra-wide range of SiO_2 (56%–71%) and clubbed them together as part of a single pluton without giving any justification. Since the Berach granite exhibit nearest temporal correlation (2540 Ma, Kaur *et al.* 2019) with the Jhiri granite (2529.6 Ma, present study), a comparison will help to understand the geochemical interrelationship of Neoarchean crust within the ADMB. In addition to Berach granite of ADMB, Neoarchean granitoids have been reported from the nearby Bundelkhand Craton. Kaur *et al.* (2016) studied 20 plutons within the Bundelkhand gneissic complex and have established presence of late Archaean (2516–2554 Ma) biotite granite in the Bundelkhand Craton. Since the Jhiri granite has similar age, the biotite granite of Bundelkhand Craton is also considered for comparison studies. The average compositional data of these plutons (table 5) show similar characteristics for major oxide composition except the higher silica content in the biotite granites of Bundelkhand craton. The classification scheme proposed by Frost *et al.* (2001) shows all three plutons are alkali-calcic, magnesian and peraluminous in nature. The Berach granite shows a significantly higher MgO content compared to the other two plutons.

The trace and REE characteristics show significant variation between the three plutons. The plot of primitive mantle normalised REEs after McDonough and Sun (1995) show an absence of Eu anomaly in case of Berach granite whereas a moderate Eu anomaly for Jhiri granite and a strong depletion for the biotite granite of Bundelkhand craton (figure 28). The same is reflected in their Eu/Eu* (table 5) values which show a range of 0.81–0.93 for Berach granite whereas the values for Jhiri granite and biotite granite of Bundelkhand craton are almost half (0.46–0.41). The flat pattern of Eu in REE spider diagram reflects primitive nature of the melt producing the Berach granite, whereas the Jhiri pluton as well as the biotite granite of Bundelkhand craton exhibits a much evolved nature. Finally, the data has been plotted in granite discrimination diagram proposed by Pearce *et al.* (1984) which show two different types where the Jhiri granite falls in the WPG field, the Berach granite and biotite granite plots in the volcanic arc granite (VAG) and syn-collisional granitoid field (Syn-colg) (figure 29). In order to further ascertain their tectonic environment, the data have been plotted in the classification scheme proposed by Whalen *et al.* (1987) which show I and S type affinity for the Berach granite and the biotite granite of Bundelkahnd craton, whereas Jhiri granite falls well within the field of A-type granite (figure 30). The I-type character of the Berach granite has been supported by the study carried out by Rahaman and Mondal (2014) and differs the interpretation made by Kaur *et al.* (2019), who have termed Berach granite as a 'biotite granite' and product of partial melting of older TTG crust. Thus the Jhiri pluton of present study shows distinct trace and REE pattern in comparison with other Neoarchean plutons. The data suggest, generation of Jhiri melt from an evolved magma compare to the Berach granite with moderate fractionation of plagioclase which is absent in case of Berach granite. Moreover, the $\varepsilon Hf(t)$ *vs.* age plot in Kaur *et al.* (2019) shows plots of Berach granite as well as majority of the Bundelkhand granites of 2.5 Ga deviate from the average continental crust trend thus interpreting partial melting of TTG crust as the only source for generation of such plutons is over simplistic and a hybrid source with contribution from a mafic melt as well as partial melting of early formed felsic crust is the most plausible explanation for generation of Neoarchean granitoids across ADMB and Bundelkhand craton.

5.3 *Stratigraphic implications*

The three sub-basins of NDT have been interpreted as rift related basin in an anorogenic setting (Sinha-Roy *et al.* 1998). The available age data of the NDT has bracketed the Delhi sedimentation as a Palaeo- to Meso-Proterozoic event (Kaur *et al.* 2007; Wang *et al.* 2017). Similar rocks in the South Delhi Fold Belt have yielded a significant younger, Neoproterozoic age (Mckenzie *et al.* 2013; Wang *et al.* 2017). Kaur *et al.* (2017) studied the intrusive plutons of the Khetri and Alwar sub-basin of NDT and suggested that Mesoproterozoic plutons (<1.8 Ga) were emplaced in a post-collisional extension settings and together with 1.8 Ga TTG crust, formed the basements for Delhi metasediments. This hypothesis was negated by the study of Wang *et al.* (2017) who have provided much older

(> 2.3 Ga for Raialo Group and > 2.1 Ga for Alwar Group) age for the cover sequence of Delhi Supergroup. Moreover, the study of Wang *et al.* (2019) suggested a period of extension during ca. 2.4 Ga and postulated that this marks the initiation of Aravalli sedimentation in the southern part of ADMB.

Present study questions the time span of the Delhi sedimentation and also the initiation of the rift systems in the northern part of Aravalli–Delhi Mobile Belt (ADMB). Presence of 2.52 Ga intrusive granitoid in the lower-most succession of the Delhi Supergroup highlights the ambiguity of the present stratigraphic classification of the host meta-sedimentaries. The meta-sedimentary sequence acted as a host to the 2.52 Ga, Jhiri pluton suggests their Archean nature and supports the idea of separate evolutionary trend (Sinha-Roy *et al.* 1998; Wang *et al.* 2017) for the northern and southern parts of ADMB. The initiation of the rift system first started in the northern part of the ADMB and corroborated later by deposition of Aravalli Group of rocks in the south. The study of Wang *et al.* (2017) shows presence of 2968 Ma age intrusive pluton within the basements, near to the contact of overlying Raialo Group. Thus, existence of 2.52 Ga intrusive granite within the Raialo Group is in concordance with periodic igneous activity in the terrane.

Synthesis of available age data across ADMB shows presence of several Neoarchean granitoids of TTG and or Sanukitoid variety in the southern part, whereas a basin scale thermal event during 1.73–1.70 Ga (Kaur *et al.* 2007, 2017) is reported in the northern part of ADMB. Present study records existence of Neoarchean granitoids in the NDT with different geochemical characteristics (A-type). Presence of 2529 Ma intrusive granite in Alwar sub-basin indicate extensional tectonic regime in northern part predates to that of southern part of ADMB. The rifting and associated basin formation was started much earlier within the NDT and probably related to the formation and breakup of earlier supercontinent cycle than Columbia (Rogers and Santosh 2002; Zhao *et al.* 2004) which is speculated to have broken up at around 1600 Ma.

6. Conclusion

The following conclusions can be drawn from the study:

- Jhiri pluton is an A-type granite, having modal composition varying from syeno-granite to quartz syenite variety with strong negative geochemical anomaly for Ba, Ta, P and Ti.
- The crystallisation age of the granite is 2529.60 ± 6 Ma which is much older than the reported granitic plutons of North Delhi Terrane (NDT).
- The existence of Neoarchean granite with dissimilar geochemical characteristics among coeval plutons of ADMB and Bundelkhand craton bear significance in respect to melt generation in different tectono-magmatic settings.
- A hybrid source, having component of fractional crystallization derived mafic melt mixing with melt generated by partial melting of early formed felsic crust in a back-arc extension or post-orogenic extension setting is proposed as the possible scenario.

Acknowledgements

The authors would like to thank Dr James Pebam, Senior Geologist, Geological Survey of India, Geochronology and Isotope Geology Division, Central Head Quarters, Kolkata for geochronological study. The authors express their gratitude to Dr Dipayan Guha, Director, Geochronology Division, Central Head Quarters, Kolkata for the help and support for providing the BSE and CL images of studied zircon. The authors also like to thank Addl. Director General and HOD, GSI, Western Region, Jaipur for all the support and help during the present study. The technical discussions and critical comments made by Dr D B Guha, ex-DDG, GSI, WR has improved the manuscript a lot. The suggestions and modifications provided by two anonymous reviewers have helped to improve the overall quality of the manuscript.

References

Abdel-Rahman A M 1994 Nature of biotites from alkaline, calc-alkaline and peraluminous magmas; *J. Petrol.* **35** 525–541.

Barbarin B 1999 A review of the relationships between granitoid types, their origin and their geodynamic environments; *Lithos* **46** 605–626.

Biju-Sekhar S, Yokoyama K, Pandit M K, Okudaira T, Yoshida M and Santosh M 2003 Late Paleoproterozoic magmatism in Delhi Fold Belt, NW India and its

implication: Evidence from EPMA chemical ages of zircons; *J. Asian Earth Sci.* **22** 89–207.

Chappel B W and White A J R 1974 Two contrasting granite types; *Pac. Geol.* **8** 173–176.

Chaudhary A K, Gopalan K and Sastry C A 1984 Present status of the geochronology of the Precambrian rocks of Rajasthan; *Tectonophys.* **105** 131–140.

Collins W J, Beams S D, White A J R and Chappell B W 1982 Nature and origin of A-type granites with particular reference to south-eastern Australia; *Contrib. Mineral. Petrol.* **80** 189–200.

Crawford A R 1970 The Precambrian geochronology of Rajasthan and Bundelkhand, northern India; *Can. J. Earth Sci.* **7** 91–110.

Dall'Agnol R, Frost C D and Rämö O T 2012 IGCP Project 510: 'A-type granites and related rocks through time': project vita, results, and contribution to granite research; *Lithos* **151** 1–16.

Deer W A, Howie R A and Zussman J 1996 *An introduction to the rock-forming minerals*; John Wiley and Sons, New York, 528p.

Duchesne J C, Berza T, Liegeois J P and Auwera J V 1998 Shoshonitic liquid line of descent from diorite to granite: The late Precambrian post-collisional Tismana pluton (South Carpathians, Romania); *Lithos* **45** 281–303.

Eby G N 1992 Chemical subdivision of the A-type granitoids: Petrogenetic and tectonic implications; *Geology* **20** 641–644.

Emslie R F 1978 Anorthosite massifs, rapakivi granites, and late proterozoic rifting of north America; *Precamb. Res.* **7** 61–98.

Foster M D 1960 Interpretation of the composition of trioctahedral micas; *USGS Prof. Paper* **354-B** 11–49.

Forster H J, Tischendorf G and Trumbull R B 1997 An evaluation of the Rb *vs.* (Y + Nb) discrimination diagram to infer tectonic setting of silicic igneous rocks; *Lithos* **40** 261–293.

Frost B R, Barnes C G, Collins W J, Arculus R J, Ellis D J and Frost C D 2001 A geochemical classification for granitic rocks; *J. Petrol.* **42** 2033–2048.

Geology and mineral resources of Rajasthan 2001 *Geol. Surv. Ind. Misc. Publ.* 2nd edn, **30** 113p.

Gupta S N, Arora Y K, Mathur R K, Iqbaluddin, Prasad B, Sahai T N and Sharma S B 1997 The Precambrian geology of the Aravalli region, southern Rajasthan and northeastern Gujarat; *Mem. Geol. Surv. India* **123** 262.

Heron A M 1917 The geology of north-eastern Rajputana and adjacent district; *Mem. Geol. Surv. India* **45** 1–128.

Heron A M 1922 Geology of western Jaipur; *Records Geol. Surv. India* **54** 345–397.

Horstwood M S A, Foster G L, Parrish R R, Noble S R and Nowell G M 2003 Common-Pb corrected *in-situ* U–Pb accessory mineral geochronology by LA-MC-ICP-MS; *J. Anal. At. Spectrom.* **18** 837–846.

Kaur P, Chaudhri N, Raczek I, Kröner A and Hofman A 2007 Geochemistry, zircon ages and whole-rock Nd isotopic systematics for Palaeoproterozoic A-type granitoids in the northern part of the Delhi belt, Rajasthan, NW India: Implications for late Palaeoproterozoic crustal evolution of the Aravalli craton; *Geol. Mag.* **144** 361–378.

Kaur P, Zeh A, Chaudhri N and Eliyas N 2016 Unravelling the record of Archaean crustal evolution of the Bundelkhand Craton, northern India using U–Pb zircon monazite ages, Lu–Hf isotope systematics, and whole-rock geochemistry of granitoids; *Precamb. Res.* **281** 384–413.

Kaur P, Zeh A, Chaudhri N and Eliyas N 2017 Two distinct sources of 1.73–1.70 Ga A-type granites from the northern Aravalli orogen, NW India: Constraints from *in-situ* zircon U–Pb ages and Lu–Hf isotopes; *Gondwana Res.* **49** 164–181.

Kaur P, Zeh A and Chaudhri N 2019 Archean crustal evolution of the Aravalli Banded Gneissic Complex, NW India: Constraints from zircon U–Pb ages, Lu–Hf isotope systematics, and whole rock geochemistry of granitoids; *Precamb. Res.* **327** 81–102.

Loiselle M C and Wones D R 1979 Characteristics and origin of anorogenic granites; *Geol. Soc. Am. Abstr. Progr.* **11** 468.

Ludwig K R 2012 Isoplot v. 3.75: A geochronological toolkit for Microsoft Excel; Special Publication, No **4**, Berkeley Geochronology Center 75.

Maniar P D and Piccoli P M 1989 Tectonic discrimination of granitoids; *Geol. Soc. Am. Bull.* **101** 635–643.

McDonough W F and Sun S-s 1995 The composition of the Earth; *Chem. Geol.* **120** 223–253.

Mckenzie N R, Hughes N C, Myrow P M, Banerjee D M, Deb M and Planavsky N J 2013 New age constraints for the Proterozoic Aravalli–Delhi successions of India and their implications; *Precamb. Res.* **238** 120–128.

Middlemost E A K 1985 Magmas and Magmatic Rocks. *An Introduction to Igneous Petrology*; London, New York: Longman, x + 266p, ISBN0582300800, *Geol. Magazine* **123(1)** 87–88, https://doi.org/10.1017/S0016756800026716.

Miller C F, Stoddard E F, Bradfish L J and Dollase W A 1981 Composition of plutonic muscovite: Genetic implications; *Canadian Mineral.* **19** 25–34.

Miller C F, McDowell S M and Mapes R W 2003 Hot and cold granites? Implications of zircon saturation temperatures and preservation of inheritance; *Geol. Soc. Am. Bull.* **31** 529–532.

Mondal M E A and Raza A 2013 Geochemistry of sanukitoid series granitoids from the Neoarchean Berach granitoid batholiths, Aravalli Craton, northwestern Indian shield; *Curr. Sci.* **105** 102–108.

Morse S A 1982 A partisan review of Proterozoic anorthosites; *Am. Mineral.* **67** 1087–1100.

Nakamura N 1974 Determination of REE, Ba, Fe, Mg, Na and K in carbonaceous and ordinary chondrites; *Geochim. Cosmochim. Acta* **38** 757–775.

Patino Douce A E 1997 Generation of metaluminous A-type granites by low-pressure melting of calc-alkaline granitoids; *Geology* **25** 743–746.

Paton C, Woodhead J D, Hellstrom J C, Hergt J M, Greig A and Maas R 2010 Improved laser ablation U–Pb zircon geochronology through robust downhole fractionation correction; *Geochem. Geophys. Geosyst.* **11** Q0AA06.

Pearce J, Harris N B W and Tindle A G 1984 Trace element discrimination diagrams for the tectonic interpretation of granitic rocks; *J. Petrol.* **25** 956–983.

Rahaman S M and Mondal M E A 2014 Evolution of continental crust of the Aravalli craton, NW India, during the Neoarchean-Palaeoproterozoic: Evidence from geochemistry of granitoids; *Int. Geol. Rev.* **57** 1510–1525.

Rogers J W and Santosh M 2002 Configuration of Columbia, a Mesoproterozoic Supercontinent; *Gondwana Res.* **5** 5–22.

Schoene B 2014 U–Th–Pb geochronology; In: *Treatise on Geochemistry* (2nd edn) Rudnick R Elsevier, Oxford, UK **4** 341–378.

Shand S J 1943 *Eruptive rocks. Their genesis, composition, classification, and their relation to ore-deposits with a chapter on meteorite.* John Wiley & Sons, New York.

Singh S P 1988 Sedimentation patterns of the Proterozoic Delhi Supergroup, northeastern Rajasthan, India, and their tectonic implications; *Sedim. Geol.* **58** 79–94.

Singh K S, Waele B D, Karmakar S, Sarkar S and Biswal T K 2010 Tectonic setting of the Balaram–Kui–Surpagla–Kengora granulites of the South Delhi Terrane of the Aravalli Mobile Belt, NW India and its implication on correlation with the East African Orogen in the Gondwana assembly; *Precamb. Res.* **18** 669–688.

Sinha-Roy S, Malhotra G and Mohanty M 1998 Geology of Rajasthan; Bangalore, *Geol. Soc. India* 278.

Sláma J, Kosler J, Condon D J, Crowley J L, Gerdes A, Hanchar J M, Horstwood M S A, Morris G A, Nasdala L, Norberg N, Schaltegger U, Schoene B, Tubrett M N and Whitehouse M J 2008 Plesovice zircon – A new natural reference material for U–Pb and Hf isotopic microanalysis; *Chem. Geol.* **249** 1–35.

Stacey J S and Kramers J D 1975 Approximation of terrestrial lead isotope evolution by a two-stage model; *Earth Planet. Sci. Lett.* **26** 207–221.

Streckeison A 1976 To each plutonic rock its proper name; *Earth-Sci. Rev.* **12** 1–33.

Sylvester P J 1989 Post-collisional alkaline granites; *J. Geol.* **97** 261–280.

Turner S, Sandiford M and Foden J 1992 Some geodynamic and compositional constraints on 'postorogenic' magmatism; *Geology* **20** 931–934.

Van-Schmus W R and Bickford M E 1981 Proterozoic chronology and evolution of the mid-continent region, North America; *Dev. Precamb. Geol.* **4** 261–296.

Vermeesch P 2018 Isoplot R: A free and open toolbox for geochronology; *Geosci. Front.* **9** 1479–1493.

Wang W, Cawood P A, Pandit M K, Zhou M F and Chen T C 2017 Zircon U–Pb age and Hf isotope evidence for an Eoarchean crustal remnant and episodic crustal reworking in response to supercontinent cycles in NW India; *J. Geol. Soc.* **174** 759–772.

Wang W, Cawood P A, Pandit M K, Zhou M F and Zhao J H 2019 Evolving passive- and active-margin tectonics of the Paleoproterozoic Aravalli Basin NW India; *Geol. Soc. Am. Bull.* **131** 426–443.

Watson E B and Harrison T M 1983 Zircon saturation revisited: Temperature and composition effects in a variety of crustal magma types; *Earth Planet. Sci. Lett.* **64** 295–304.

Wetherill G W 1956 Discordant uranium–lead ages; *Trans. Am. Geophys. Union* **37** 320–326.

Whalen J B, Currie K L and Chappell B W 1987 A-type granites: Geochemical characteristics, discrimination and petrogenesis; *Contrib. Mineral. Petrol.* **95** 407–419.

White W M, Albarède F and Télouk P 2000 High-precision analysis of Pb isotopic ratios using multi-collector ICPMS; *Chem. Geol.* **167** 257–270.

Wiendenbeck M, Allé P, Corfu F, Griffin W L, Meier M, Oberli F, Von Quadt A, Roddick J C and Spiegel W 1995 Three natural zircon standards for U–Th–Pb, Lu–Hf, trace element and REE analyses; *Geostand. Newslett.* **19** 1–23.

Zhao G, Sun M, Wilde S A and Li S 2004 A Paleo-Mesoproterozoic supercontinent: Assembly, growth and breakup; *Earth-Sci. Rev.* **67** 91–123.

Corresponding editor: Rajneesh Bhutani